Research papers

Catchment scale simulations of soil moisture dynamics using an equivalent cross-section based hydrological modelling approach

Urooj Khan[a,b], Hoori Ajami[a,c], Narendra Kumar Tuteja[b], Ashish Sharma[a,*], Seokhyeon Kim[a]

[a] School of Civil and Environmental Engineering, University of New South Wales, Sydney, New South Wales, Australia
[b] Water Forecasting Services, Bureau of Meteorology, Canberra, Australian Capital Territory, Australia
[c] Department of Environmental Sciences, University of California, Riverside, CA, United States

ABSTRACT

Physically based distributed hydrological models are useful for simulating the spatial distribution of hydrologic fluxes across the catchment under various climate and land cover change scenarios. However, complexities associated with their implementation at large scales make their applications limited. Previously, an equivalent cross-section (ECS) based distributed hydrological modelling approach was developed for first order sub-basins to reduce the computational time/effort. Here, the ECS approach is modified for semi-distributed hydrological modelling at the catchment scale. The modelling approach is implemented for a 314 km² McLaughlin catchment located in south-eastern New South Wales (NSW), Australia that consists of 822 first order sub-basins. A 26 year long streamflow record simulated using an ECS based modelling approach are compared against daily observed streamflow and four calibrated lumped conceptual hydrologic models, and found to be consistent. Further, the simulated actual evapotranspiration and soil moisture from the ECS approach are compared against the Australian Water Availability Project (AWAP) model simulations and results found to be consistent. In addition, the temporal dynamics of simulated soil moisture from the ECS approach is consistent with the satellite derived European Space Agency Climate Change Initiative (ESA CCI) surface soil moisture data. In the ECS based semi-distributed modelling, all parameters are derived from the actual topographic and physiographic information of the catchment and none of the parameters is calibrated. Therefore, this approach has the advantage of simulating streamflow in ungauged catchments compared to lumped conceptual models. The impact of spatially distributed climatic forcing and land cover on soil moisture is investigated across four landforms (upslope, midslope, footslope and alluvial-flats) and at various soil depths. Our results show increase of mean soil moisture in shallow layers of upslope toward alluvial-flats. However, mean soil moisture in deeper horizons remained almost constant across all landforms. The variability of daily soil moisture at surface soil layers is higher than the deeper soil layers for all landforms. Our results illustrated that disaggregation of a catchment to a series of ECS at the scale of first order sub-basins, captures dynamics of soil moisture and actual evapotranspiration across the landscape and results are consistent with the climatology, land cover type, topography and soil hydraulic properties. Further, the use of ECS approach in the McLaughlin catchment reduced the number of computational units by 40 times in comparison to 3-d grid based distributed modelling setup.

1. Introduction

The development and applications of physically based distributed hydrological models have increased in the last two decades, due to substantial improvements in Geographical Information System (GIS), spatial resolution of topographic, physiographic and remote sensing data, and computational power (Abbott et al., 1986a,b; Abbott and Refsgaard, 1996; Bell et al., 2007; Beven and Kirkby, 1979; Kampf and Burges, 2007; Reed et al., 2004; Singh and Woolhiser, 2002; Tague and Band, 2004; Watson et al., 1998; Wigmosta et al., 1994). During this period several distributed hydrological models are developed with various level of complexity including MIKE-SHE (Abbott et al., 1986a,b), HYDRUS-1d, 2-d & 3d (Simunek et al., 1999, 2005, 2006), CATHY (Paniconi et al., 2003), GSSHA (Downer and Ogden, 2004), MODHMS (Panday and Huyakorn, 2004), ParFlow (Kollet and Maxwell, 2006), Grid to Grid (G2G) (Bell et al., 2007; Cole and Moore, 2009), and HydroGeosphere (Brunner and Simmons, 2012). In these models parameters for every grid cell or hydrologic response units are derived

from spatially distributed data such as topography, soil type, land cover, climate and geology. In turn, spatially distributed fluxes, including transpiration, soil evaporation, deep drainage, runoff and soil moisture are obtained across the catchment. These extensive spatial fluxes from distributed models are useful for assessing the impact of climate, land use and land cover changes. On the other end, the lumped conceptual models are also very popular in hydrological modelling due to their simple structure and limited parameter requirements (Beven, 2012; Kirchner, 2006; Singh, 1995; Singh and Woolhiser, 2002). The lumped conceptual models consider entire catchment as a single unit and simulate discharge at the catchment outlet as a function of lumped representation of catchment storage.

Refsgaard and Knudsen (1996) compared the performance of three hydrological models, including a fully distributed model MIKE-SHE (Abbott et al., 1986a,b), a semi-distributed model WATBAL (Knudsen et al., 1986) and a lumped conceptual model NAM (Nielsen and Hansen, 1973). They concluded that distributed models performed better than lumped conceptual models in cases where no calibration was allowed and long term streamflow data were not available. However, often simpler conceptual models are preferred over their distributed counterparts due to significant computational effort of distributed hydrologic models for long term simulations in large catchments or due to the lack of high resolution spatial information about model parameters (Beven, 1989, 2001; Grayson et al., 1992b; Kirchner, 2006).

One possible option for reducing the computational effort/time in distributed hydrological modelling is to disaggregate the catchment into the smaller homogeneous spatial entities (Argent et al., 2007; Beven and Kirkby, 1979; Flugel, 1995; Reggiani et al., 1999; Reggiani et al., 1998; Summerell et al., 2005; Vertessy et al., 1993; Watson et al., 1999; Wood et al., 1988). These spatial entities are known with various names, including Hydrologic Response Units (HRUs) (Flugel, 1995), Representative Elementary Areas (REAs) (Wood et al., 1988), Representative Elementary Watersheds (REWs) (Reggiani et al., 1998) and Functional Units (FUs) (Argent et al., 2007), with the term HRUs being commonly used in hydrology. Wood et al. (1988) delineated REAs on the basis of topography, soil and rainfall. Flugel (1995) and Argent et al. (2007) developed the concept of HRUs and FUs on the basis of similarities in topographical and physiographical features of the catchment.

Most of the existing methods of catchment disaggregation, either lack contiguity and topological connectivity of HRUs, or require artificial nodes to connect these entities, which restricts the transfer of lateral fluxes from the upper part of a hillslope to the lower parts. To address this, Khan et al. (2013) developed an approach to delineate contiguous topologically connected HRUs to transfer the fluxes from the upper parts of a hillslope to the lower parts. To delineate HRUs, the entire catchment was divided into four major landforms (upslope, midslope, footslope and alluvial-flats). Four landforms were delineated on the basis of similarities in topographical and geomorphological attributes of a catchment. The catchment was also divided into different stream order sub-basins based on Strahler's convention, ensuring that the variability of saturated hydraulic conductivity was least in first order sub-basins. Following the HRU delineation, Khan et al. (2014) developed an equivalent cross-section (ECS) approach for semi-distributed hydrologic modelling at the scale of first order sub-basins, where landform-based delineated HRUs were used as the basis for weighting the topographical and physiographical features of first order sub-basins. As HRUs are embedded in the ECS formulation, ECSs are capable of transferring fluxes from the upper parts of a hillslope to the lower parts. The Soil Moisture And Runoff simulation Toolkit (SMART) developed by Ajami et al. (2016) also used ECS approach.

In the ECS approach, either single or multiple ECSs were formulated as a weighted representation of a first order sub-basin depending on the arrangement of soil types within the sub-basin. Water balance simulations for these ECSs are performed using a 2-d distributed hydrological model. The ECS approach was investigated for eight first order sub-basins and modelling results showed that it was effective for reducing the computational time/effort in a 2-d distributed hydrological modelling without significant loss of accuracy in simulated fluxes (Khan et al., 2014). Despite considerable improvement in computational efficiency of the ECS approach in comparison to distributed cross section modelling approaches, performance of the ECS approach at a catchment scale with multiple first order sub-basins was not investigated in Khan et al. (2014). Further, no verification of simulated stream flow against observations was performed due to non-availability of streamflow observations at the first order sub-basin scale, which serves as the motivation of the current study.

The aims of this study are to; 1) modify the ECS approach for semi-distributed hydrological modelling at the catchment scale which contains 822 first order sub-basins, 2) compare simulated streamflow of a calibration free ECS approach with observations, and simulations from four calibrated lumped conceptual models and 3) examine soil moisture dynamics for the entire catchment and across four landforms at various soil depths under different climate and land cover types.

2. Study area

This study is conducted for the McLaughlin catchment, which is a sub-catchment of the Snowy River located in the Snowy Monaro region in south-eastern New South Wales (NSW), Australia. The total catchment area of the McLaughlin up to the confluence of Snowy River is 459 km². The catchment area up to the gauging station is used in this study due to the availability of observed streamflow at the gauging station. The McLaughlin catchment up to the gauging station (Fig. 1a) has the area of 314 km² and consists of 822 first order sub-basins. The first order sub-basins areas vary from 0.8 ha to 283 ha. The elevation range in the McLaughlin catchment up to the gauging station varies from 740 m to 1231 m. The McLaughlin catchment is considered in this study because this catchment and its neighbouring catchments have been under hydrologic investigation for the last ten years because of changes in land cover during the last 50 years (Khan et al., 2013; Tuteja et al., 2007).

The Digital Elevation Model (DEM) data has the resolution of 25 m × 25 m and is derived from the contour and drainage data of NSW topographic maps. All data for this research was taken from the previous studies by Tuteja et al. (2007).

2.1. Climate and runoff

Four climate zones were delineated for the McLaughlin and its neighbouring catchments by Teng et al. (2008) using the climate surfaces of the Australian continent developed by Jeffrey et al. (2001) (Fig. 1b). The daily Scientific Information for Land Owners (SILO) climate surfaces use daily gauged climate data of approximately 4600 locations across Australia. The density of these climate stations varies across Australia. The density of climate stations is high near the coast of Australia, especially in the south-east where the McLaughlin catchment is located. The SILO climate surfaces use spatial interpolation algorithms to generate daily climate surfaces such as daily rainfall and evaporation at 5 km × 5 km spatial resolution (Jeffrey et al., 2001). The Root Mean Square Error (RMSE) of monthly SILO rainfall for 1990–1997 was 35.1 mm (Jeffrey et al., 2001).

In McLaughlin and its neighbouring catchments, the range of annual rainfall, mean annual rainfall and pan evaporation for four climate zones delineated by Teng et al. (2008) for the period 1975–2000 are presented in Table 1. The mean annual rainfall and pan evaporation for the McLaughlin catchment for the period 1975–2000 are 658 mm/y and 992 mm/y respectively. The annual rainfall for the McLaughlin catchment for a wet year (1978) and a dry year (1982) varies in the range 1041 mm/y and 370 mm/y respectively, and the respective annual pan evaporation values are 933 mm/y and 1194 mm/y. Daily streamflow
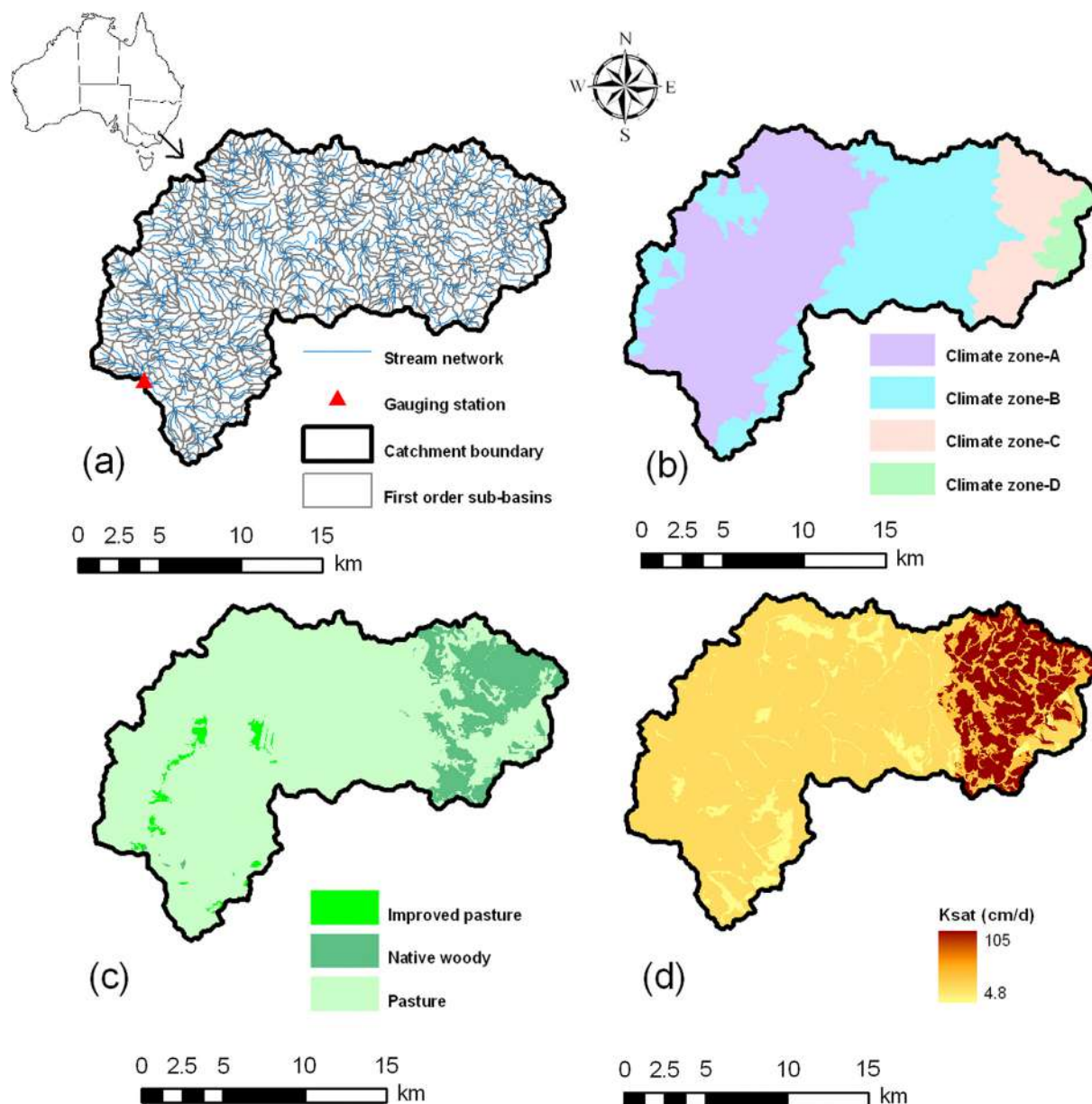
Fig. 1. a) Catchment map showing first order sub-basins and stream network, b) Climate zone map (A: < 600 mm/y; B: 600–750 mm/y; C: 750–900 mm/y and D: > 900 mm/y), c) Land cover map and d) Saturated Hydraulic Conductivity (Ksat) map of top soil horizon/material of the McLaughlin catchment.

Table 1
Climate data summary for four climate zones.

Climate zones	Range of annual rainfall (mm/y)	Mean annual rainfall for the period 1975–2000 (mm/y)	Mean annual pan evaporation for the period 1975–2000 (mm/y)
A	< 600	551	1038
B	600–750	662	977
C	750–900	825	930
D	> 900	1300	817

data for the period 1975–2000 at the gauging station is used in this study with the mean annual streamflow of 85 mm/y, which is significantly lower than the rainfall, indicating most of the rainfall is lost to evapotranspiration.

The delineation of four climate zones used in this study is validated by comparing the range of annual rainfall in four climate zones with the average annual rainfall from SILO grid cells. The average annual rainfall for 1975–2000 period are calculated for all 26 SILO grid cells of size 5 km × 5 km located either partly or fully in the McLaughlin catchment (Fig. S-1 in the Supplementary material). The rainfall pattern at gridded scale matches closely with the rainfall pattern of four climate zones (Fig. 1b). This analysis confirms that the delineation of climate zones is correct and the spatial variation of rainfall is well represented by these climate zones.

2.2. Land cover

The McLaughlin catchment mainly consists of three land cover types i.e. pasture, native woody and improved pasture (Tuteja et al., 2006) (Fig. 1c), out of which pasture and native woody are the dominant land cover types, comprising 86% and 13% of the total area respectively. The area under improved pasture is negligible and therefore this land cover class is merged with the pasture in this study. The Leaf Area Index (LAI) and root biomass distributions of pasture and native woody land cover types are taken from Tuteja et al. (2006, 2007).

2.3. Soil type and depth

Murphy et al. (2005) developed a soils information package for the McLaughlin and neighbouring catchments, which comprises spatial distribution of soil types, soil depth and soil hydraulic properties on the basis of their respective parent material, ancillary data sources and field observations. Murphy et al. (2005) categorized individual soil types on the basis of similarities in metadata associated with each soil type (e.g. particle size analysis, bulk density and water holding capacity). The soil hydraulic properties were determined using Pedotransfer Function (PTF) models of Minasny and McBratney (2002) and Schaap and Leij (1998). The soil types map and soil hydraulic properties of the McLaughlin catchment are presented in Fig. S-2 and Table S-1 respectively of the supplementary material. On the basis of this data, a 25 m × 25 m pixel size raster of saturated hydraulic conductivity (Ksat) of the top soil horizon/material is generated (Fig. 1d) for the McLaughlin catchment. The variation of Ksat is in the range of 4.8 cm/d to 105 cm/d. These values are inferred on the basis of soil physical properties (e.g. particle size distributions and bulk density), soil topo-sequences, extensive field work and laboratory analysis (Chapman and Atkinson, 2000; Geeves et al., 1995; Murphy et al., 2005). While acknowledging uncertainty around Ksat values, we note that these are high quality soils data sets for large catchments.

Soil depth data is taken from Murphy et al. (2005) based on the methodology of McKenzie et al. (2003). The soil depths are higher near valley bottoms and lower at the top of hillslopes.

3. Catchment modelling

Semi-distributed modelling using the ECS approach consists of the following steps: 1) delineating first order sub-basins, 2) delineating HRUs using topographic and geomorphic analysis of the entire catchment, 3) ECS delineation, 4) 2-dimensional soil moisture model simulations across every ECS in a first order sub-basin, and 5) post processing of outputs. The description of 2-dimensional soil moisture movement model, HRUs and ECS approach, and catchment modelling methodology are presented in the following sub-sections.

3.1. 2-Dimensional Richards' equation based unsaturated soil moisture movement model

The unsaturated soil moisture movement model (U3M-2d) developed by Tuteja et al. (2004) is used to perform the hydrological modelling across the ECSs of the McLaughlin catchment. This model is based on the 2-d solution of Richards' equation. The Richards' equation has been criticised for simulating the hydrologic fluxes at coarse scale as it was originally derived at point scale (Beven, 2001; Beven, 2012; Grayson et al., 1992a; Grayson et al., 1992b; Kirchner, 2006; Singh and Woolhiser, 2002), and may not capture non-linearity of hydrological processes at various scales. However, still majority of existing physically based distributed hydrological models use the Richards' equation (either1-d, 2-d or 3-d formulation) to calculate unsaturated zone fluxes. These models include: MIKE-SHE (Abbott et al., 1986a; Abbott et al., 1986b), HYDRUS-1d, 2-d & 3d (Simunek et al., 1999, 2005, 2006), CATHY (Paniconi et al., 2003), GSSHA (Downer and Ogden, 2004), MODHMS (Panday and Huyakorn, 2004), tRIBS + VEGGIE (Ivanov et al., 2008a,b), ParFlow (Kollet and Maxwell, 2006), and HydroGeosphere (Brunner and Simmons, 2012). Previous investigations have shown that these models have been successful in simulating the hydrological fluxes at catchment scale. The Richards' equation based U3M-2d model has also been successful in simulating the hydrological fluxes from the ECSs (Khan et al., 2014).

The U3M-2d model is an extended version of 1-d unsaturated soil moisture movement model (U3M-1d) developed by Vaze et al. (2004), which was based on 1-d solution of Richards' equation. The detailed concept and equations used in U3M-2d are presented in Section

3.11–3.13 of Tuteja et al. (2004) (see http://www.toolkit.net.au/Tools/CLASS-U3M-1D/publications for details).

The model requires four types of input data for each modelling element (pixel): 1) climate, which includes daily rainfall, pan evaporation, maximum and minimum temperature and radiation, 2) soil hydraulic properties and soil depths, 3) root biomass distribution and leaf area index (LAI) of each land cover types, and 4) elevation and slope of each pixel. U3M-2d divides the entire soil column into four soil horizons or soil materials, and each soil material is further divided into thinner soil layers for computational purpose. The model uses three boundary conditions, 1) specified flux (rainfall minus potential soil evaporation) at the soil surface, 2) free drainage boundary condition at the bottom of the soil profile; specified head or specified flux boundary condition is also available in the model for the bottom of the soil profile, and 3) specified flux representing soil moisture contribution from upslope pixels across each soil material of the soil profile.

The U3M-2d model uses Richards' equation for performing local water balance computations along the vertical axis (for each soil layer) of every pixel of a hillslope cross section while accounting for flux from the upslope areas. Gravity drainage, capillary rise, evapotranspiration, soil moisture and downslope soil water outflow are then computed for each pixel. A variable sub-daily time step is used for partitioning the water balance (transpiration, soil evaporation, deep drainage and soil moisture excess) in the unsaturated zone. The sub-daily computational time step varies from user defined minimum (e.g. 5 min) to maximum (e.g. 1 hr) and exact values are decided on the basis of rainfall intensity. The smaller time step (e.g. 5 min) is considered for the very high intensity rainfall (e.g. 1000 mm/d) and 1 hr time step for the low intensity rainfall (e.g. 5 mm/d). For rainfall intensity in between these two extremes, the time steps are adaptively adjusted depending on the transient soil moisture conditions. To calculate rainfall intensity at a sub-daily time step, U3M-2D disaggregates the input daily rainfall data by dividing the daily rainfall with the user defined time step, used in the vertical water balance calculation. For example, an hourly time step is used for low rainfall intensity of 5 mm/d.

Potential plant transpiration and potential soil evaporation are calculated from potential evapotranspiration on the basis of monthly LAI and land cover type. Actual transpiration and soil evaporation are dynamically calculated on the basis of available water in the root zone, user defined root biomass distribution and transpiration factor derived from the wilting point, field capacity and saturated soil moisture contents.

The horizontal water balance component of U3M-2d model performs the computations at daily time scale. The excess moisture arising from the variably saturated conditions within each soil material is aggregated at a daily time scale and horizontally transferred to the respective soil materials in the next downslope pixel based on Darcy's law. The daily simulated fluxes for each pixel are soil moisture, actual transpiration, soil evaporation, horizontal fluxes and drainage below the root zone (deep drainage).

3.2. Overview of sub-basin, HRU and equivalent cross-section delineation approach

Catchment modelling starts with dividing the catchment into Strahler's first order sub-basins. The order of sub-basins was decided on the basis of variation in saturated hydraulic conductivity of soils as sub-basins are aggregated to higher units, i.e., second and higher order sub-basins. Results from Khan et al. (2013) showed significant increases in saturated hydraulic conductivity variability in higher order sub-basins. Therefore, first order sub-basins are selected as units for aggregating and transferring hydrologic fluxes down the stream. Within a first order sub-basin, contiguous, topologically connected HRUs are delineated to transfer the soil moisture fluxes from the upper parts of a hillslope to the lower parts. Khan et al. (2013) derived landform delineation thresholds from a range of terrain analysis techniques – the Cumulative

Area Distribution (CAD) curve, average local slope, curvature, Compound Topographic Index (CTI) and the Multi Resolution Valley Bottom Flatness (MRVBF) index and divided the catchment into four major landforms (upslope, midslope, footslope and alluvial flats). These landforms represent the macroscopic changes in the catchment landscapes. The widths of alluvial flats, footslope, midslope and upslope are: 0–25 m, 25–75 m, 75–350 m and > 350 m respectively for the McLaughlin catchment. Note that, the delineated landform widths are smaller near the stream network and increases with distance from the stream in order to represent the saturation zone more appropriately near the stream network.

These HRUs were used as the basis for formulating the ECS approach at the first order sub-basin scale to reduce the computational time/effort in distributed hydrological modelling, without significant reduction in accuracy (Khan et al., 2014). To formulate an ECS, multiple cross sections are delineated in a sub-basin and then the topographical and physiographical features of cross sections are length weighted averaged on a landform basis within a sub-basin. Depending on the soil type pattern, single or multiple ECS in each Strahler's first order sub-basin were formulated to represent the full or a part of the sub-basin. Soil type pattern within a sub-basin determine the number of ECS as follows: 1) If the soil types remain unchanged within a sub-basin, then a single equivalent cross-section can represent the entire sub-basin, 2) If the soil types are consistent with landform pattern, i.e., different soil near the center of the river and changes towards the ridge line, then the three equivalent cross-sections, left bank, right bank and head water, can represent a sub-basin, and, 3) If the soil types do not follow a landform pattern or any other systematic pattern, at least one equivalent cross-section in each soil type is required to represent a sub-basin. Khan et al. (2014) investigated the ECS approach for seven discrete first order sub-basins of the McLaughlin catchment along with the Wagga-Wagga experimental catchment. The simulated fluxes from the ECS approach were compared with the simulated fluxes from the distributed modelling at multiple cross-sections. The fluxes obtained from both approaches were very close whereas the computational time reduced significantly using the ECS approach. As observed streamflow data for the first order sub-basins were not available, the ECS approach was validated using soil moisture observations in the Wagga-Wagga experimental catchment and results found to be consistent with the observed soil moisture (Khan et al., 2014). The Soil Moisture And Runoff simulation Toolkit (SMART) developed by Ajami et al. (2016) used ECS approach. Here, the ECS approach is modified to perform semi-distributed hydrological modelling at the catchment scale and to compare the simulated runoff with the observed discharge at the catchment outlet.

3.3. Catchment scale modelling using the equivalent cross-sections with four landforms

A summary of the ECS formulation with four landforms (ECS-4LF) for catchment scale modelling is presented in Fig. 2. As can be seen in Fig. 2a, a sample first order sub-basin contains four landforms: upslope, midslope, footslope and alluvial flats to maintain topological connectivity in a hillslope. The McLaughlin catchment contains 822 first order sub-basins (Fig. 1a) with variety of soil types (Fig. S-2 in Supplementary material and Fig. 1d). To formulate the ECS for 822 first order sub-basins in an automated manner, it is essential to maintain consistency in ECS formulation approach throughout all sub-basins. Therefore, all ECS are formulated on the basis of soil types and landforms. For example, if the first order sub-basin has three soil types (Fig. 2b), three ECS (one each for each soil type) are formulated (Fig. 2c) and in the case of one soil type, only a single ECS is formulated for the entire sub-basin.

To formulate ECSs on a four landform basis (ECS-4LF), first order sub-basins layer of the catchment is overlaid with the soil type and landform layers (Fig. 3). Therefore, each first order sub-basin will contain soil type polygons and within each soil polygon, landforms are available. One ECS-4LF is formulated for each soil type polygon within each first order sub-basin (Fig. 3). To perform the 2-d distributed hydrologic modelling on each ECS-4LF, the following topographical and physiographical parameters are required for each pixel of the ECS-4LF: elevation, soil depths, slope, climate, land cover and soil type. The following parameters are calculated for each landform of the ECS: width, slope, elevation, land cover and climate.

To compute landform width, it is assumed that the shape of each landform polygon is rectangular. This is a reasonable assumption because the actual landforms are generally long narrow curvy strips and they can be replicated by equal area/perimeter rectangles (Fig. 2a & 3). Eq. (1) is used to calculate the width of each landform within a soil polygon using its area and perimeter:

$$w_i = \frac{p_i - \sqrt{p_i^2 - 16a_i}}{4} \tag{1}$$

where,

$i = 1$ (upslope), 2 (midslope), 3 (footslope) and 4 (alluvial flats)

w_i is the width of landform i and a_i and p_i are the area and perimeter of the landform i respectively calculated in ArcGIS. The 2-d distributed hydrological modelling of an ECS-4LF is performed along the length of an ECS-4LF obtained by summation of the widths of all landforms, i.e. upslope, midslope, footslope and alluvial flats, within a soil polygon. Note that, Khan et al. (2014) calculated the length of an ECS by arithmetic averaging of the lengths of multiple cross-sections drawn in a first order sub-basin. Drawing of multiple cross-sections in each first order sub-basin is not practically feasible here as the number of sub-basins is large (822) and the ECS formulation needs to be automated. Therefore, calculation of ECS-4LF length is simplified for formulating the ECS-4LF in 822 first order sub-basins. The length of an ECS-4LF is divided into 25 m interval, i.e., the resolution of DEM data, and model parameters are obtained for each element.

Average slope of each landform within a soil polygon is obtained by averaging local slope of all grid cells (25 m × 25 m) in a landform. Local slope is calculated in ArcGIS using available DEM data, and the average landform slope is used in formulating an ECS-4LF (Fig. 3). In a similar manner, average soil depths of all four soil materials/horizons for each landform are calculated from the available soil depth rasters of individual soil material/horizons (Fig. 3). Note that, Khan et al. (2014) calculated the slope and soil depth of each landform of an ECS by length weighted averaging of slope and soil depth of multiple cross-sections drawn in a first order sub-basin. But as stated above, drawing of multiple cross-sections in each first order sub-basin is not practically feasible due to number of sub-basins. Therefore, calculation of slope and soil depth is simplified here.

For the climate and land cover type, only the dominant class in each landform within a soil polygon of a first order sub-basin is obtained. For example, if 80% area of a landform is covered with pasture and 20% covered with native woody, then the pasture land cover is assigned for this landform and the associated 25 m pixels (Fig. 3).

The maximum elevation of each landform is calculated from the DEM data. This elevation was assigned to the first upslope pixel of the uppermost landform in an ECS-4LF. The elevations of other pixels in the ECS-4LF are calculated with the help of average slope of landforms and landform widths which are calculated earlier (Fig. 3).

The land cover types, climate zones, soil depths of all soil materials and slopes are considered constant within those pixels of an ECS-4LF that are located within the same landform. For example if an ECS-4LF is 250 m long (10 pixels), and upslope contains 3 pixels, then the land cover type (dominant), climate zone (dominant), soil depth (average) and slope (average) of these 3 pixels remain the same. In this manner, a total of 2392 ECSs-4LF are formulated for 822 first order sub-basins in the McLaughlin catchment. The 2-d distributed hydrological modelling
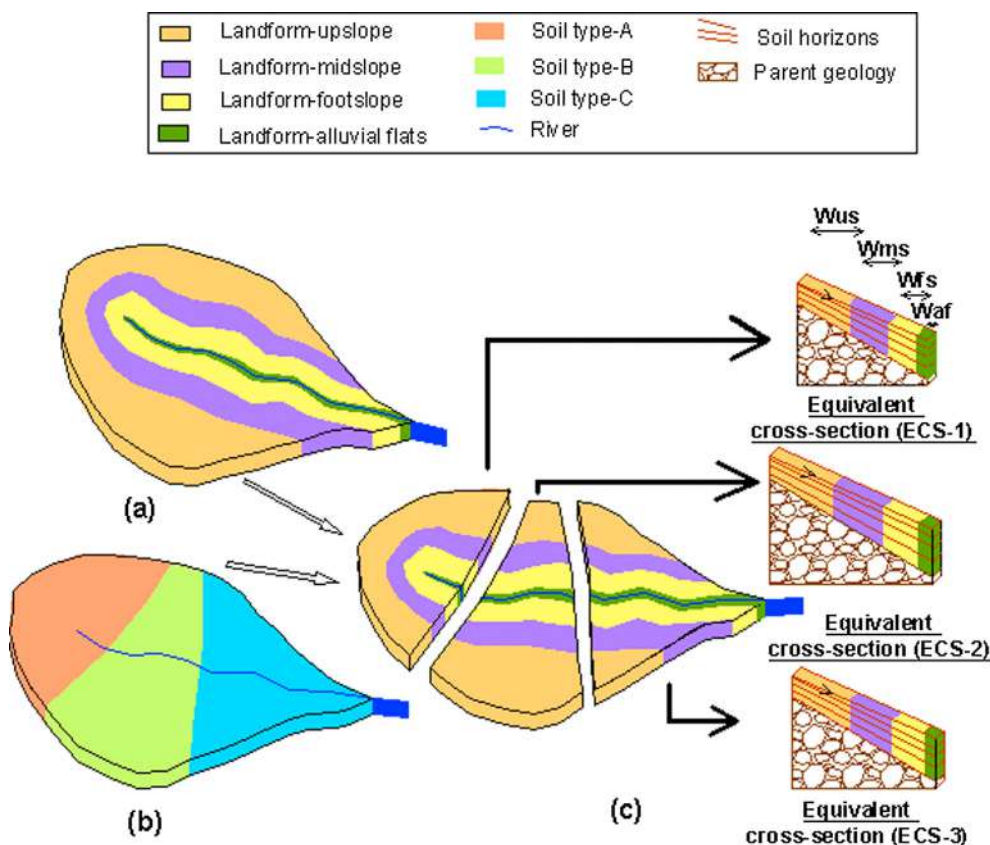
is performed for every ECS-4LF using the U3M-2d at a pixel scale. The connectivity of first order sub-basins with stream network is shown in Fig. 1a. The simulated results are available for each pixel of an ECS-4LF and it includes daily soil moisture, actual transpiration, soil evaporation, horizontal fluxes and drainage below the root zone (deep drainage).

Initial processing of the topographical and physiographical data for formulating an ECS-4LF is performed in ArcGIS and the final output organized in an attribute table which contains ECS properties. Later, R and Matlab scripts are written to process this data and prepare input data files in an automated manner for the U3M-2d model. The soil hydraulic properties and land cover related parameters are also assigned in input files using R and Matlab scripts. The U3M-2d model written in C#, run for 2392 ECS-4LF using a workflow based approach which is written in R. The simulated data is post processed using R scripts.

3.4. Catchment scale modelling using the equivalent cross-sections with single landform

To investigate the impact of aggregating ECS properties in simulated fluxes, the four landforms of an ECS are replaced with a single landform. The method of formulating and processing of geospatial data in the equivalent cross-section on a single landform basis (ECS-SLF) is similar to the ECS-4LF. The major difference is on the averaging/weighting of topographical and physiographical properties of an ECS is performed on a single landform instead of four landforms.

As one ECS-SLF is delineated per soil polygon, the average slope of all grid cells in a soil polygon is calculated as there is only one landform within a soil polygon. In a similar manner, average soil depths of all four soil materials/horizons for each soil polygon are calculated from the available soil depth rasters of individual soil material/horizons. For the climate and land cover type, only the dominant class in each soil polygon of a first order sub-basin is obtained. For example, if 80% area

of a soil polygon is covered with pasture and 20% covered with native woody, then the pasture land cover is assigned for this single landform and the associated 25 m pixels.

To compute the single landform width, the soil polygons are assumed to be an equivalent square, and the width of a square is calculated by taking the square root of soil polygon area. This is a reasonable assumption as areas of polygons are preserved here compared to the ECS-4LF and the equivalent square concept helps in automating ECS formulation in large catchments.

The maximum elevation of each soil polygon is calculated from the DEM and was assigned to the first upslope pixel of an ECS-SLF. The elevations of other pixels in the ECS-SLF are calculated with the help of the average slope of a single landform and landform width calculated earlier.

The land cover types, climate zones, soil depths of all soil materials and slopes are considered constant within each pixel of single landform. For example if a single landform is 250 m long (10 pixels), then the land cover type (dominant), climate zone (dominant), soil depth (average) and slope (average) of these 10 pixels remain the same. Note that, in this example the length of ECS-SLF will also be 10 pixels as there is only one landform in each ECS. In this manner, a total of 2458 ECSs-SLF are formulated for 822 first order sub-basins in the McLaughlin catchment. Simulations across ECS-SLF are performed using the U3M-2D at pixel scale as described in Section 3.3. Note that, the U3M-2d model remains unaltered in both the ECS-4LF or ECS-SLF approaches presented here. In each case the model is applied at a pixel scale with parameters derived for four or a single landform depending on whether the ECS-4LF or ECS-SLF approach is considered.

3.5. Catchment modelling using lumped conceptual models

In the ECS-4LF and ECS-SLF based distributed modelling approaches, actual topographical and physiographical parameters were obtained from the geospatial data without any calibration. To compare
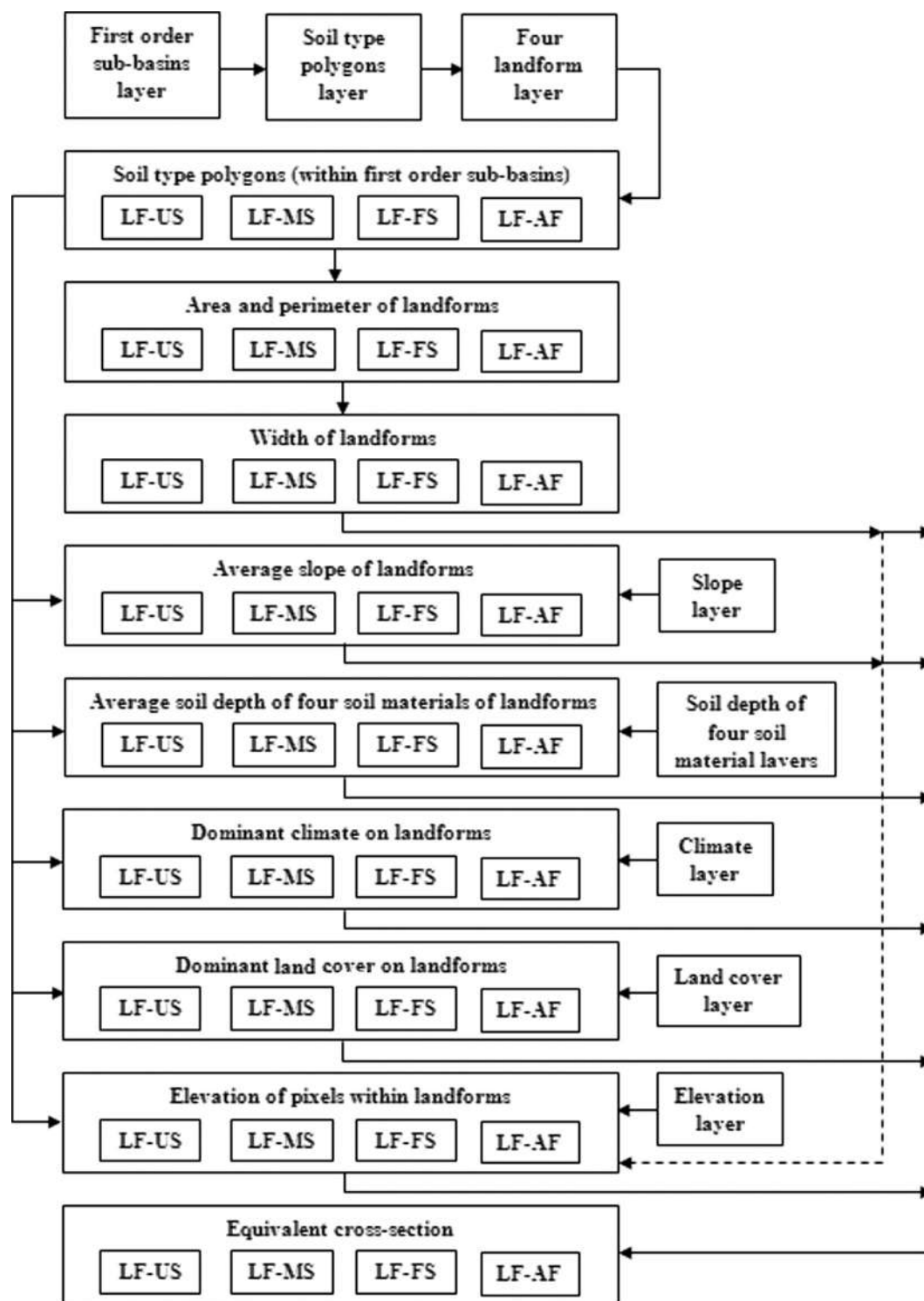
Fig. 3. Flow chart of the equivalent cross-section formulation. Landform-upslope (LF-US), Landform-midslope (LF-MS), Landform-footslope (LF-FS) and Landform-alluvial flats (LF-AF).

the ECS-4LF and ECS-SLF based modelling simulations against lumped conceptual models which require thorough calibration, four lumped conceptual models, GR4J, Sacramento, Simhyd and SMAR in different setups are used.

3.5.1. GR4J

A four parameter based lumped conceptual model GR4J developed by Perrin et al. (2003) is used within WAFARi2 (Water Availability Forecast of Australian Rivers) modelling system which is the modified

version of WAFARi, developed by the Bureau of Meteorology, Australia, to issue seasonal streamflow forecasts (Shin et al., 2011; Tuteja et al., 2011). The GR4J model is selected because of its high performance in simulating streamflow for a wide range of Australian catchments. The GR4J model is calibrated for each year in cross-validation mode for the period 1970–2000 using a 5-year leave out window. As an example, when simulating streamflow for 1981, GR4J is calibrated using data for 1970–1980 and 1986–2000. Similarly, the 5-years moving leave out window steps through all years during 1970–2000. Altogether, 200

parameter sets are generated by using a weighted least square (WLS) option for the total error model to define the objective function in the Bayesian Total Error Analysis (BATEA) framework within the WAFARi2 modelling system (Kavetski et al., 2006a,b; Shin et al., 2011; Tuteja et al., 2011). Generated parameter sets for each year are used in the model to generate 200 ensembles of daily streamflow for each year with the observed daily rainfall and evaporation data. The differences between these 200 ensembles are negligible and therefore median, mean or even a single ensemble member gives the same results. In this study, median of 200 ensembles is considered for each year, and a continuous daily time series of simulated streamflow for the entire study period, i.e. 1975–2000, is generated using the McLaughlin daily rainfall and potential evapotranspiration data.

3.5.2. Sacramento, Simhyd and SMAR simulations

Three lumped conceptual models, Sacramento (Burnash, 1985; Burnash et al., 1973), Simhyd (Chiew et al., 2002) and SMAR (Kachroo, 1992; O'Connell et al., 1970; Tuteja and Cunnane, 1999) are also specified for the McLaughlin catchment to compare with the simulations from the ECS-4LF and ECS-SLF cases. These widely used lumped models are specified by dividing the entire data length (1975–2000) into two equal parts for model calibration (1975–1987) and validation (1988–2000). The 1970–1974 simulation period is considered as the warm-up period. The computer programs for all three models (Sacramento, Simhyd and SMAR) are obtained from the Rainfall Runoff Library (RRL) (Podger, 2004). Model calibration is performed using the Shuffled Complex Evolution method (SCE-UA) (Duan et al., 1993, 1994) and Nash Sutcliffe Efficiency (NSE) (Nash and Sutcliffe, 1970) is used as the objective function. A continuous daily time series of simulated streamflow for the entire study period (i.e. 1975–2000) is generated using the optimized parameters for each model.

3.6. WaterDyn/AWAP model for evapotranspiration and soil moisture verification

The WaterDyn model was developed under the Australian Water Availability Project (AWAP) by CSIRO (Raupach et al., 2009). The WaterDyn/AWAP model is a terrestrial water balance model runs at 5 km × 5 km grid scale and solves the water balance equations mainly in unsaturated soil columns at a daily time step (Raupach et al., 2009). To verify the simulated evapotranspiration from the ECS-4LF and ECS-SLF approaches, simulated monthly evapotranspiration from the WaterDyn model is used as no eddy covariance or sap flux data is available. The spatial variation of average annual evapotranspiration and soil moisture for the entire study period (1975–2000), wet year (1978) and dry year (1982) from the WaterDyn/AWAP model are also compared with the ECS-4LF and ECS-SLF approaches. The results are presented and discussed in Section 4.2.3.

3.7. Satellite derived data for soil moisture verification

The European Space Agency Climate Change Initiative (ESA CCI) surface soil moisture data are used to verify simulated soil moisture from the ECS-4LF approach. The ESA CCI has released daily surface (~2 cm) soil moisture products at a spatial resolution of 0.25° (approximately 25 km at Equator) using seven passive and three active microwave spaceborne instruments covering 38 years from November 1, 1978 to December 31, 2016 (current version 04.2) (http://www.esa-soilmoisture-cci.org/) (Liu et al., 2012). Three products are available in the CCI soil moisture: active, passive, and active–passive combined data, which have been comprehensively validated at the global scale and applied for long-term studies with promising performances (Dorigo et al., 2017; Kim et al., 2018; Miralles et al., 2013). The ESA CCI soil moisture is a composite product from the multiple passive and active microwave spaceborne instruments, and there have been advances in the quality and temporal coverage of the product through time. The

1979–1987 data product is based on a single instrument, while the 1991–2000 data are from the multiple advanced instruments (Chung et al., 2018). Further, the number of observations in each year is high during 1991–2000 period in comparison to the 1979–1987 period. There are no observations available during Aug-1987 to Jul-1991 period in ESA CCI soil moisture data set covering the study catchment. Considering the significant differences in quality and number of observations in ESA CCI soil moisture data set during 1979–1987 and 1991–2000 periods, the 1991–2000 data set is used in this study. From the ESA CCI soil moisture data, area weighted catchment average daily soil moisture is generated for the McLaughlin catchment. This data is compared with the landform area weighted catchment average daily simulated soil moisture from the top model layer (10 cm) in the ECS-4LF approach. The results are presented and discussed in Section 4.2.4.

4. Results and discussion

The comparison of simulated streamflows from the ECS-4LF and ECS-SLF approaches with the observed streamflow and four conceptual models are presented in the following sub-sections. The spatial distribution of hydrological fluxes and analysis of soil moisture dynamics for different climates and different land covers of the entire catchment and landforms, from the ECS-4LF and ECS-SLF approaches are also presented.

4.1. Comparison of simulated and observed streamflows

The daily time series of simulated streamflows from all models and approaches are compared with the observed streamflows in the following sub-section. Further, the scatter between the simulated and observed streamflows and bias are also compared in the following sub-sections.

4.1.1. Comparison of daily flow series for a selected year

Daily horizontal fluxes and deep drainage are simulated for each pixel of an ECS-4LF and ECS-SLF using the U3M-2d model. The deep drainage from all the pixels in ECS-4LF and ECS-SLF are arithmetically averaged and added with the horizontal fluxes from the last pixel to obtain the total streamflow from the single ECS-4LF and ECS-SLF. Total streamflow from every ECS is multiplied by the soil polygon area from which the ECS-4LF or ECS-SLF was formulated to obtain weighted total streamflow for a first order sub-basin. The weighted total daily streamflow from all 822 sub-basins are added to obtain the total simulated streamflow at the outlet of McLaughlin catchment. Simulated daily streamflow from the ECS approach and four conceptual models (GR4J, Sacramento, Simhyd and SMAR) are shown for the year 1995 as it is one of the validation years for the lumped conceptual models (Fig. 4a-f). The Nash Sutcliffe Efficiency (NSE) and Mean Absolute Error (MAE) values for the entire simulation period, i.e., 1975–2000 at daily, monthly and annual time scales are presented in Tables 2and 3 respectively. The daily NSE of the ECS-4LF simulation is lower than all four conceptual models (Tables 2). However, at the monthly time scale, performance of the ECS-4LF approach is improved and is comparable with other conceptual models (Tables 2). At annual time scale, the ECS-4LF approach has the second highest NSE after the Sacramento model (Tables 2). Daily, monthly and annual NSE values of the ECS-4LF approach are higher than the ECS-SLF approach. The daily MAE of the ECS-4LF approach is very low, and only the MAE of GR4J is lower than the ECS-4LF approach (Table 3). The monthly and annual MAE values of ECS-4LF approach are higher than the Sacramento and SMAR models, close to GR4J model, and lower than the Simhyd model (Table 3). The MAE values of ECS-SLF at daily, monthly and annual scale are higher than the ECS-4LF approach (Table 3). It should be noted that the NSE values are more influenced by accurately simulating high flows whereas MAE reflect the overall performance, i.e., high as well as low flows. As a result, it can be concluded that the overall
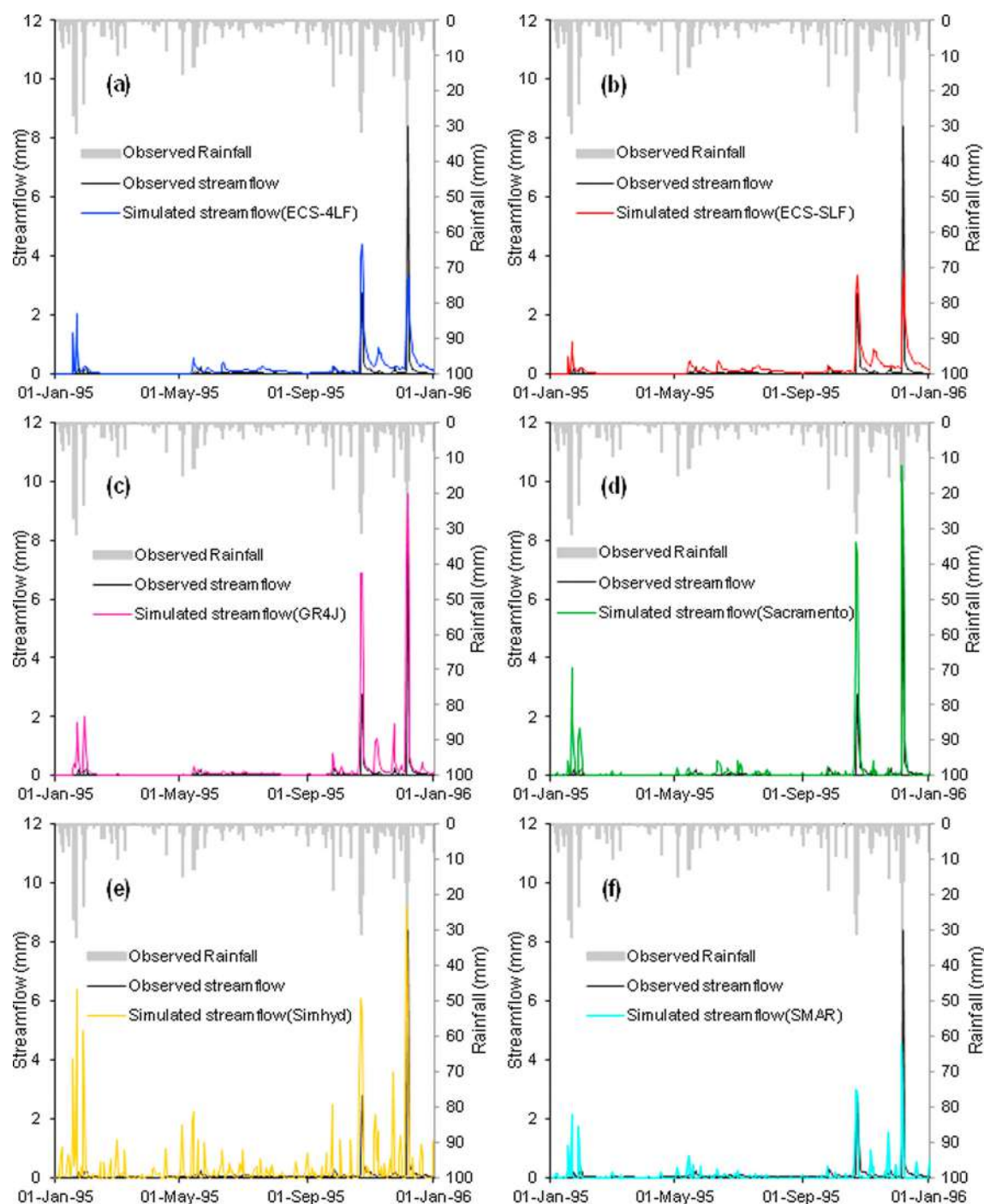
Fig. 4. Daily time series of observed and simulated streamflows from the a) ECS-4LF, b) ECS-SLF, c) GR4J, d) Sacramento, e) Simhyd and f) SMAR for the year 1995.

Table 2
Comparison of NSE values of all models at daily, monthly and annual time scales for the period 1975–2000.

Modelling approaches/Models	NSE-daily	NSE-monthly	NSE-annual
ECS-4LF	0.32	0.54	0.68
ECS-SLF	0.23	0.47	0.64
GR4J	0.43	0.55	0.60
Sacramento	0.53	0.67	0.74
Simhyd	0.41	0.65	0.35
SMAR	0.59	0.70	0.67

Table 3
Comparison of Mean Absolute Error (MAE) values of all models at daily, monthly and annual time scales for the period 1975–2000.

Modelling approaches/ Models	MAE-daily (mm)	MAE-monthly (mm)	MAE-annual (mm)
ECS-4LF	0.21	4.75	39.72
ECS-SLF	0.24	5.27	42.48
GR4J	0.19	4.57	39.21
Sacramento	0.23	4.10	29.71
Simhyd	0.38	6.81	65.15
SMAR	0.24	3.74	34.40

performance of the ECS-4LF approach is reasonable, given no calibration is involved in its specification, and this approach has the potential to be applied in ungauged areas.

At a daily time scale the ECS-4LF and ECS-SLF approaches simulate low flows well (Fig. 4a-f) while underestimating the very high flow events (Fig. 4a-b). Performance of conceptual models for streamflow simulation varies. The GR4J model overestimates high flows in 1995 but simulates low flows with reasonable accuracy (Fig. 4c). The Sacramento and Simhyd models overestimate high and low flows in 1995 (Fig. 4d and e). The SMAR model simulates low as well as high flows reasonably well but it underestimates a few high flow events in 1995 (Fig. 4f). The performance of ECS-4LF at a daily time scale is reasonable by considering that no parameter adjustment is performed for this approach and all parameters are directly derived from the topographical and physiographical features of the catchment.

4.1.2. Overall model performance comparison

The bias of daily simulated streamflow is calculated by estimating the average difference between the simulated and observed streamflows for the entire period (1975–2000). The positive bias indicates overestimation of streamflows by the model and negative bias indicates underestimation. The ECS-4LF, ECS-SLF and GR4J models have small bias during low flows whereas high negative bias exists for some of the high flow events (Fig. 5a-c). The Sacramento model has mostly positive bias in low and high flows and it overestimates some of the high flow events (Fig. 5d). The Simhyd model significantly overestimates low and high flows as shown by a large positive bias throughout the simulations (Fig. 5e). The bias in SMAR is slightly smaller than the other five models during low and high flow periods (Fig. 5f). Though none of these models perform extraordinarily well, all conceptual models require observed streamflows to optimise parameter sets, which is not the case with ECS-4LF and all parameters are directly derived from the topographical and physiographical features of the catchment. As a result, it can be concluded that the ECS-4LF approach can be applied in ungauged catchments with reasonable accuracy.

Water balance partitioning based on ECS-4LF approach revealed that the actual evapotranspiration constitutes around 82% of rainfall for the whole study period, whereas the deep drainage and horizontal flows constitute around 15% and 2% respectively of rainfall. Therefore, the majority of rainfall evapotranspires and only a small amount of rainfall contributes to streamflow. Previously, Khan et al. (2014) performed 2-d distributed modelling on multiple cross-sections on seven first order sub-basins. Properties of these cross sections are derived from actual topographic and physiographic properties of each pixel in a cross section. Comparison of simulated soil moisture and various hydrological fluxes including transpiration and soil evaporation from the ECS approach found to be consistent with these distributed cross section simulations. In particular, simulated evapotranspiration from the ECS approach closely resembles distributed cross section simulations. We further assess accuracy of simulated evapotranspiration using data from the Australian Water Availability Project (Raupach et al., 2009) presented in Section 4.2.

To analyse sensitivity of streamflow to initial soil moisture conditions, two extreme initial conditions, very wet (close to saturation) and very dry (close to residual moisture content), are considered in the ECS-4LF approach. The ECS-4LF simulations with average initial soil moisture conditions are presented throughout this paper. Comparison of three simulated streamflow time series from the wet, dry and average initial condition with daily observed streamflow shows that the initial soil moisture conditions cause small differences in simulated streamflows for the first few (8–9) months. After that, the impact of initial condition diminishes and all three simulated time series become similar (figures are not presented here but are available from the authors on request).

One of the major benefits of the ECS-4LF with U3M-2d model approach over the conceptual models is that it provides a variety of spatially distributed hydrological fluxes in addition to streamflow, whereas the conceptual models only provide catchment average outputs. The various spatially distributed hydrological fluxes will be discussed in the following sections.

In comparison with the 3-d grid based distributed modelling approaches, the number of modelling elements decreased substantially, from 501,953 pixels for a 3-d case to 12,430 pixels for the ECS-4LF approach in the McLaughlin catchment. This 40 times reduction in the number of computational units is irrespective of CPU speed and decreases the computational time at the same order, i.e., 40. This reduction in computational units/time will enable hydrologic modellers to assess long term climate change impacts in large catchments using high resolution spatial information and also to perform uncertainty analysis using multiple climate change scenarios.

The impact of channel routing on simulated streamflow from the ECS-4LF approach is also explored. Three routing models are applied at the catchment scale. These are the Muskingum model (Cunge, 1969; Nash, 1959), Ordinary Least Square (OLS) model (Liang and Nash, 1988) and Linear Perturbation Model (LPM) (Nash and Barsi, 1983). To apply these models, single input and single output routing schemes are considered and parameters of the routing models are calibrated using the observed streamflow data. While adding these routing models slightly improved simulated streamflow, the results were not consistent throughout the study period. As a result, the routing models were not considered due to calibration of routing parameters. In addition, channel routing becomes important in catchments that are larger than the study catchment (Liang and Nash, 1988). For those very large catchments, calibration free channel routing models can be developed similar to those used for ungauged areas. All simulation results presented here are based on derived parameter values from the actual topographical and physiographical features of the catchment and no calibration was performed. As channel routing is not considered in the ECS-4LF and ECS-SLF approaches, water storage mechanism in channels cannot be considered. However, the impacts of unsaturated zone storage on streamflow and the rest of catchment fluxes are considered in the U3M-2d model.

4.2. Spatial variability of catchment scale fluxes in relation to climate and land cover

Daily actual transpiration and soil evaporation are simulated on each pixel of an ECS-4LF and ECS-SLF using the U3M-2d model. The actual transpiration and soil evaporation are added to calculate daily actual evapotranspiration. For the ECS-4LF approach, actual evapotranspiration values for each landform within a soil polygon were obtained as an arithmetic average of pixels located in the same landform inside a soil polygon of a first order sub-basin. In the ECS-SLF approach, as there is only a single landform in each soil polygon, the actual evapotranspiration values were obtained as an arithmetic average of pixels located inside a soil polygon of a first order sub-basin. Fig. 6a and 7a present the spatial variation of average annual evapotranspiration from the ECS-4LF approach (at landform scale) and ECS-SLF approach (at soil polygon scale) respectively, across the McLaughlin catchment for the period 1975–2000. Daily soil moistures are simulated for each pixel of an ECS-4LF and ECS-SLF at various depths. To obtain mean annual soil moisture for each landform within a soil polygon for the ECS-4LF approach, the soil moisture values of all pixels in a given landform are averaged for the duration of the analysis. In a similar manner, for the ECS-SLF approach, the soil moisture values of all pixels in a soil polygon are averaged for the duration of the analysis to obtain mean annual soil moisture for each soil polygon. Results are only presented for the surface soil layer of 10 cm depth (Fig. 6d for ECS-4LF and 7d for ECS-SLF). The averaging of pixel values in a given landform will result in uniform soil moisture and evapotranspiration values in a landform. Because the alluvial flat landform width is 0–25 m, saturation in soil moisture generally occurs near the stream network. The width of
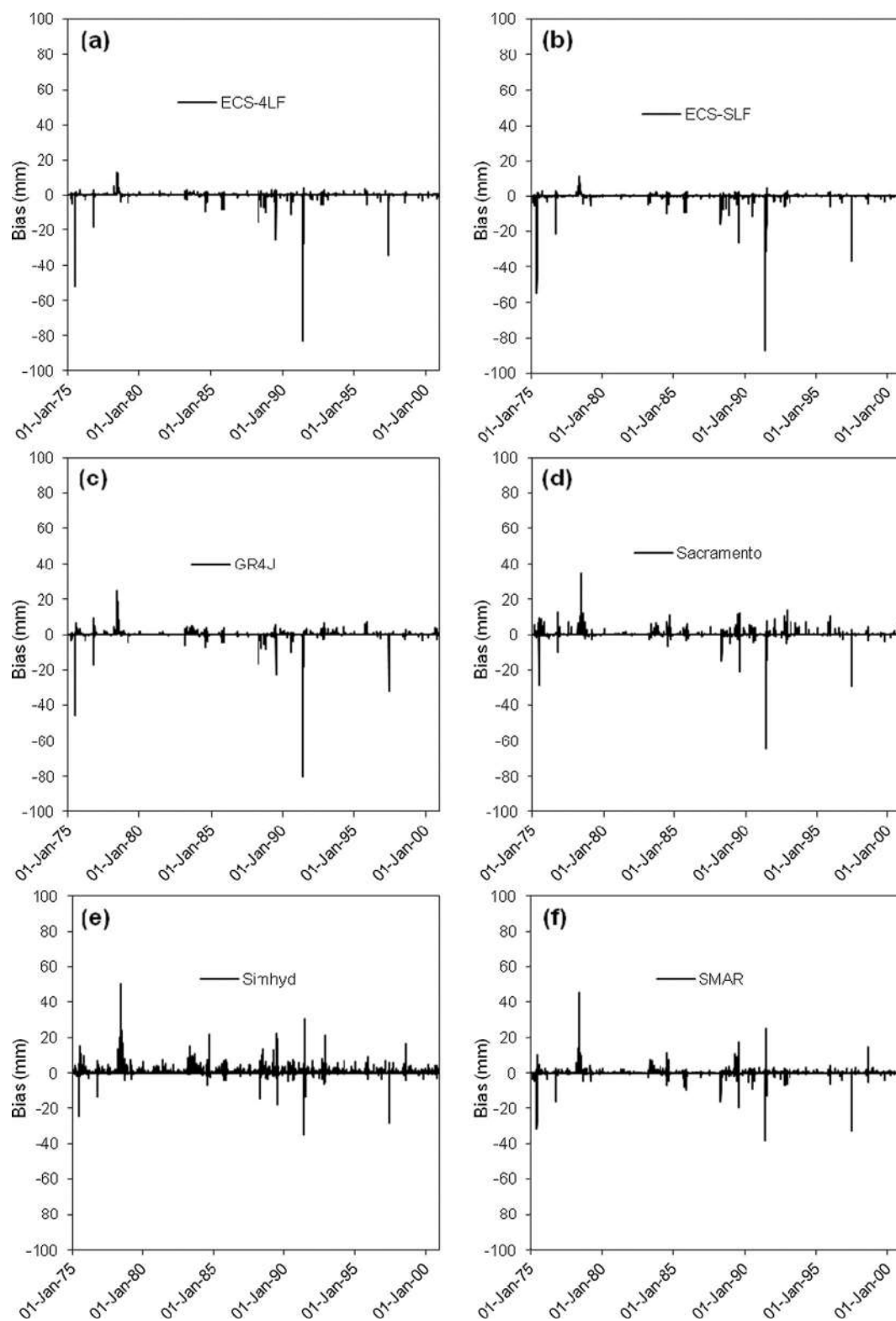
Fig. 5. Daily bias in streamflows simulated from a) ECS-4LF, b) ECS-SLF, c) GR4J, d) Sacramento, e) Simhyd and f) SMAR for the entire period (1975–2000).

footslope is 50 m (25 m to 75 m from the stream network), therefore this landform will show average soil moisture of two pixels in the ECS-4LF approach.

To compare the soil moisture distribution across a wet and a dry year, average wet year (1978) and dry year (1982) soil moisture values for the ECS-4LF and ECS-SLF are also mapped in Figs. 6e-f & 7e-f respectively. Further, the spatial pattern of evapotranspiration in a wet

(1978) versus a dry year (1982) for ECS-4LF and ECS-SLF approaches are presented in Figs. 6b-c & 7b-c respectively.

4.2.1. Spatial variability of evapotranspiration

Simulated average annual evapotranspiration in the McLaughlin catchment ranges from 414 mm/y to 682 mm/y for the ECS-4LF and 426 mm/y to 680 mm/y for the ECS-SLF approach (Figs. 6a & 7a). The
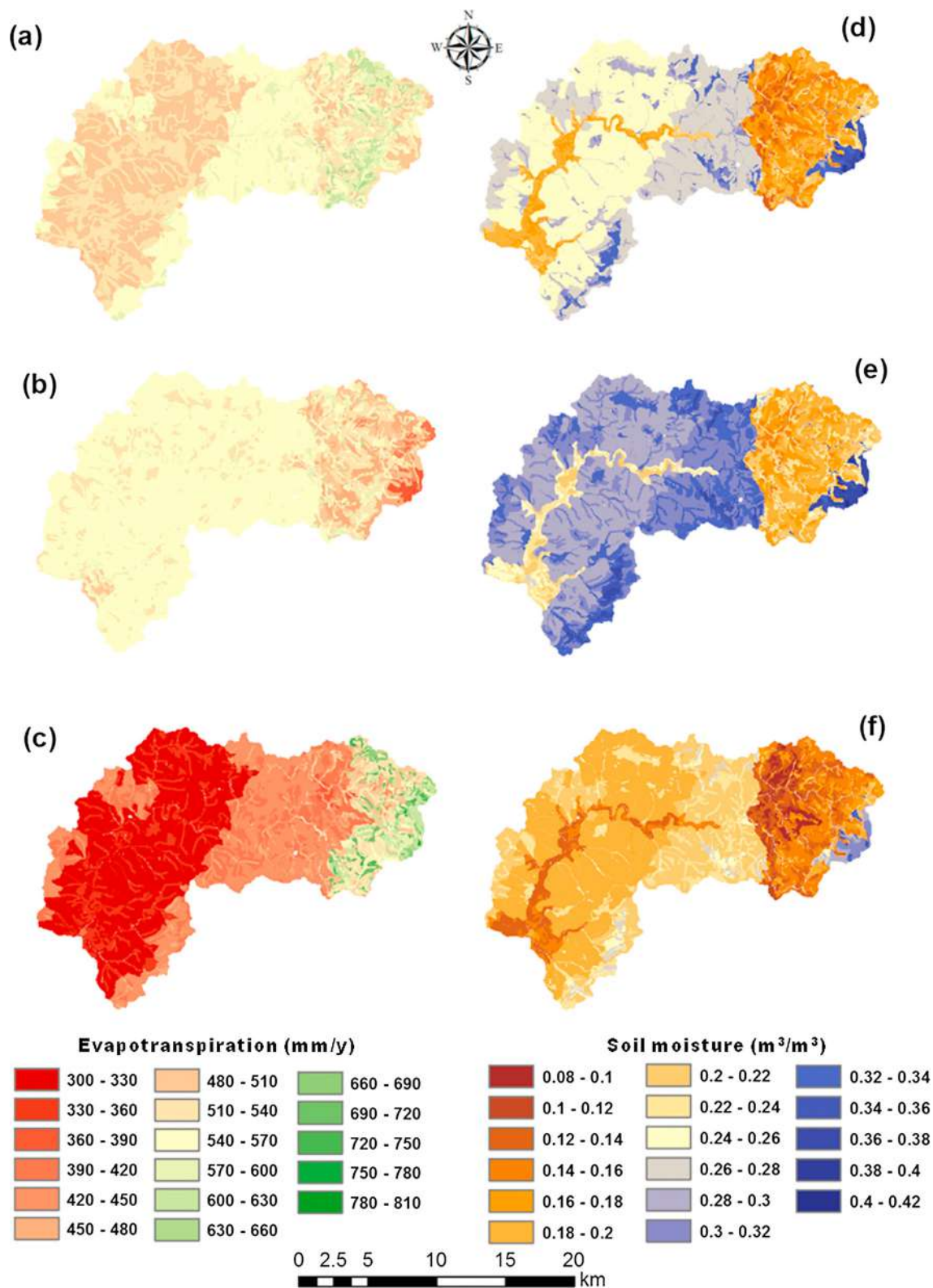
Fig. 6. Simulated actual evapotranspiration and soil moisture from the ECS-4LF approach for the McLaughlin catchment, a) average annual evapotranspiration, b) wet year (1978) evapotranspiration, c) dry year (1982) evapotranspiration, d) average soil moisture at surface soil layer for the whole study period (26 yr), e) wet year (1978) average soil moisture at surface soil layer and f) dry year (1982) average soil moisture at surface soil layer.

ranges of average annual evapotranspiration in both ECS approaches are very close but the ECS-SLF range is slightly narrower because the averaging of topographical and physiographical properties is done at the soil polygon scale instead of four landforms in a sub-basin. On average, evapotranspiration for native woody and pasture land cover types are 555 mm/y and 538 mm/y respectively for the ECS-4LF approach whereas these are 557 mm/y and 537 mm/y respectively for ECS-SLF approach. Evapotranspiration is higher for the native woody

compared to the pasture due to higher water use efficiency, e.g. higher LAI and deeper roots of the native woody vegetation (Figs. 6a, 7a & 1c).

Mean annual evapotranspiration in a wet year varies between 367 mm/y to 628 mm/y for the ECS-4LF approach and 371 mm/y to 627 mm/y for the ECS-SLF approach. The rainfall and potential evapotranspiration are 1041 mm/y and 793 mm/y respectively (Jeffrey et al., 2001; Teng et al., 2008) (Figs. 6b & 7b). The maximum evapotranspiration in both ECS-4LF and ECS-SLF approaches are lower than the potential evapotranspiration in a wet year due to higher frequency of anoxic condition caused by fully saturated conditions in the root zone. Despite the higher rainfall in the upper part of the catchment compared to the low land, the evapotranspiration is lower due to the lower potential evapotranspiration in climate zones C & D (Table 1) and frequency of anoxic conditions.

Mean annual evapotranspiration in a dry year varies between 304 mm/y to 807 mm/y for the ECS-4LF approach and 311 mm/y to 805 mm/y for ECS-SLF approach (Fig. 6c & 7c). The evapotranspiration in a dry year strongly shows the pattern of climate zones (rainfall) for ECS-4LF and ECS-SLF approaches (Fig. 6c, 7c & 1b, Table 1). The rainfall amount in a dry year is very low, i.e., 370 mm/y, and potential evapotranspiration is high, i.e., 1015 mm/y. Therefore, actual evapotranspiration is highly controlled by the limited available water in a dry year. The upper ranges of evapotranspiration in the dry year for both ECS-4LF and ECS-SLF approaches are higher than the wet year because the potential evapotranspiration in the dry year is significantly higher (1015 mm/y) than the wet year (793 mm/y) (Fig. 6b-c & 7b-c).

A common trend found in the first order sub-basins of all evapotranspiration maps in the ECS-4LF approach (Fig. 6a-c), is that evapotranspiration is gradually increasing from the upper landforms, i.e., upslope, toward the bottom landform, i.e., alluvial flats. However, this trend is not presented in evapotranspiration maps of ECS-SLF approach because the entire soil polygon is treated as one landform (Fig. 7a-c). Therefore, the ECS-4LF approach is superior to the ECS-SLF approach in representing the spatial variation of evapotranspiration along the hillslopes. The increasing trend of evapotranspiration from the upper landform to the bottom landform is consistent with the field scenarios as evapotranspiration is high in the wetter zones located close to the river network. Further, it is also consistent with the increasing trend in soil moisture from the upper landforms to bottom landforms as discussed in the next section, which shows that the evapotranspiration is highly controlled by the amount of available water in the root zones.

In both ECS-4LF and ECS-SLF approaches, most of the evapotranspiration occurs in shallow rooting pasture as it covers around 86% of the entire catchment and the remainder is the native woody covering 13% of the catchment. The simulated evapotranspiration from the ECS-4LF is very close to the ECS-SLF approach but the ECS-SLF approach is unable to simulate the evapotranspiration at a landform scale. Note that the evapotranspiration is the dominant flux in the McLaughlin catchment. The comparison of simulated evapotranspiration from ECS-4LF and ECS-SLF approaches with the simulated evapotranspiration from WaterDyn model (Raupach et al., 2009) is presented in detail in Section 4.2.3.

4.2.2. Spatial variability of soil moisture

The average soil moisture maps for ECS-4LF and ECS-SLF approaches for the whole study period, wet year and dry year show lower soil moisture values in the upper part of the catchment and in few areas of the lower part of the catchment (Figs. 6d-f & 7d-f). In the upper part of the catchment, soil moisture values are lower because of higher evapotranspiration from the native woody and the presence of shallow yellow earth granite and earthy sands granite soil types. In these soil types, surface soil material has significantly higher saturated hydraulic conductivity than the deeper soil materials, causing more water to move down in the deeper soil materials and retain less water in the surface soil material (Fig. 1c, d and Fig. S-2 in Supplementary material). The lower values of soil moisture in few areas of the lower part of the

catchment such as along the main stem of the river network are mostly due to the dominance of Lithosols Metasediments soil type (Figs. 6d-f, 7d-f, 1d and Fig. S-2 in Supplementary material). The saturated hydraulic conductivity (Ksat) of Lithosols Metasediments is 24 cm/d in all four soil horizons/materials (Table S-1 in the Supplementary material). These high values of Ksat in the lower soil horizons/materials allow more water to pass downwards as deep drainage and less moisture is retained in top soil layers (Figs. 6d-f, 7d-f, 1d and Fig. S-2 in Supplementary material). Further, all soil moisture maps in ECS-4LF and ECS-SLF approaches closely reflect soil types and climate zones pattern (Figs. 6d-f, 7d-f, 1b, d and Fig. S-2 in Supplementary material). In particular, the soil type pattern dominates because the soil type plays an important role for simulating the water balance and soil moisture values.

The average surface soil moisture for the ECS-4LF and ECS-SLF during the whole study period (26 yr) varies from 0.12 (m^3/m^3) to 0.41 (m^3/m^3) over the entire catchment. For the wet year (1978), this ranges between 0.14 (m^3/m^3) to 0.42 (m^3/m^3) (Figs. 6d-e and 7d-e). For the dry year (1982), the average soil moisture for the ECS-4LF varies from 0.09 (m^3/m^3) to 0.37 (m^3/m^3) and for the ECS-SLF varies from 0.09 (m^3/m^3) to 0.36 (m^3/m^3) (Figs. 6f and 7f). As can be seen in these figures, no significant differences between the ECS-4LF and ECS-SLF simulations are observed when ranges of soil moisture for the whole duration, wet year or dry year are considered. As it is expected, soil moisture values are higher in a wet year compared to the dry year for both ECS-4LF and ECS-SLF approaches throughout the catchment, reflecting the influence of input rainfall and potential evapotranspiration (Figs. 6e-f & 7e-f). In the ECS-4LF approach, all three soil moisture maps show that the bottom landforms, i.e., alluvial flats, have higher soil moisture values compared to the rest of the landforms because of higher saturation near the river network (Fig. 6d-f). This pattern is not visible in some sub-basins in the lower part of the catchment especially along the main stem of the river network (Fig. 6d-f). Low soil moisture values in these regions are due to the prevalence of Lithosols Metasediments soil type that allows more deep drainage and less moisture retained in the top soil layers (Fig. 6d-f and Fig. S-2 in Supplementary material). Small water content of the top soil layer in all four landforms (upslope, midslope, footslope and alluvial flats) of the main river network results in small variation of soil moisture in these landforms during wet and dry periods (Fig. 6d-f). The increase in soil moisture near the river network cannot be seen in soil moisture maps from the ECS-SLF approach as the entire soil polygon is treated as a single landform (Fig. 7d-f). This highlights the importance of using multiple landforms in the ECS approach to simulate the spatial variability of land surface states and fluxes. The variability of soil moisture across landforms in the ECS-4LF approach will be discussed in detail in Section 4.3.

Note that, the spatial variation of evapotranspiration and soil moisture cannot be simulated in lumped conceptual models as the entire catchment is treated as a single unit. This highlights the importance of using the ECS-4LF based semi-distributed modelling approach. The spatial comparison of simulated soil moisture from ECS-4LF and ECS-SLF approaches with the simulated soil moisture from WaterDyn model (Raupach et al., 2009) is presented in the next section.

4.2.3. Verification of evapotranspiration and soil moisture from WaterDyn/AWAP model

The monthly simulated evapotranspiration values for 1975–2000 period are extracted from the WaterDyn/AWAP model developed by Raupach et al. (2009) for the grids which are either completely or partly located in the McLaughlin catchment. The weighted monthly evapotranspiration is calculated for the entire McLaughlin catchment from these gridded data and compared with the ECS-4LF and ECS-SLF simulated evapotranspiration (Fig. 8a-b). The simulated evapotranspiration from both ECS-4LF and ECS-SLF approaches are very close to the WaterDyn/AWAP model throughout the simulation period.

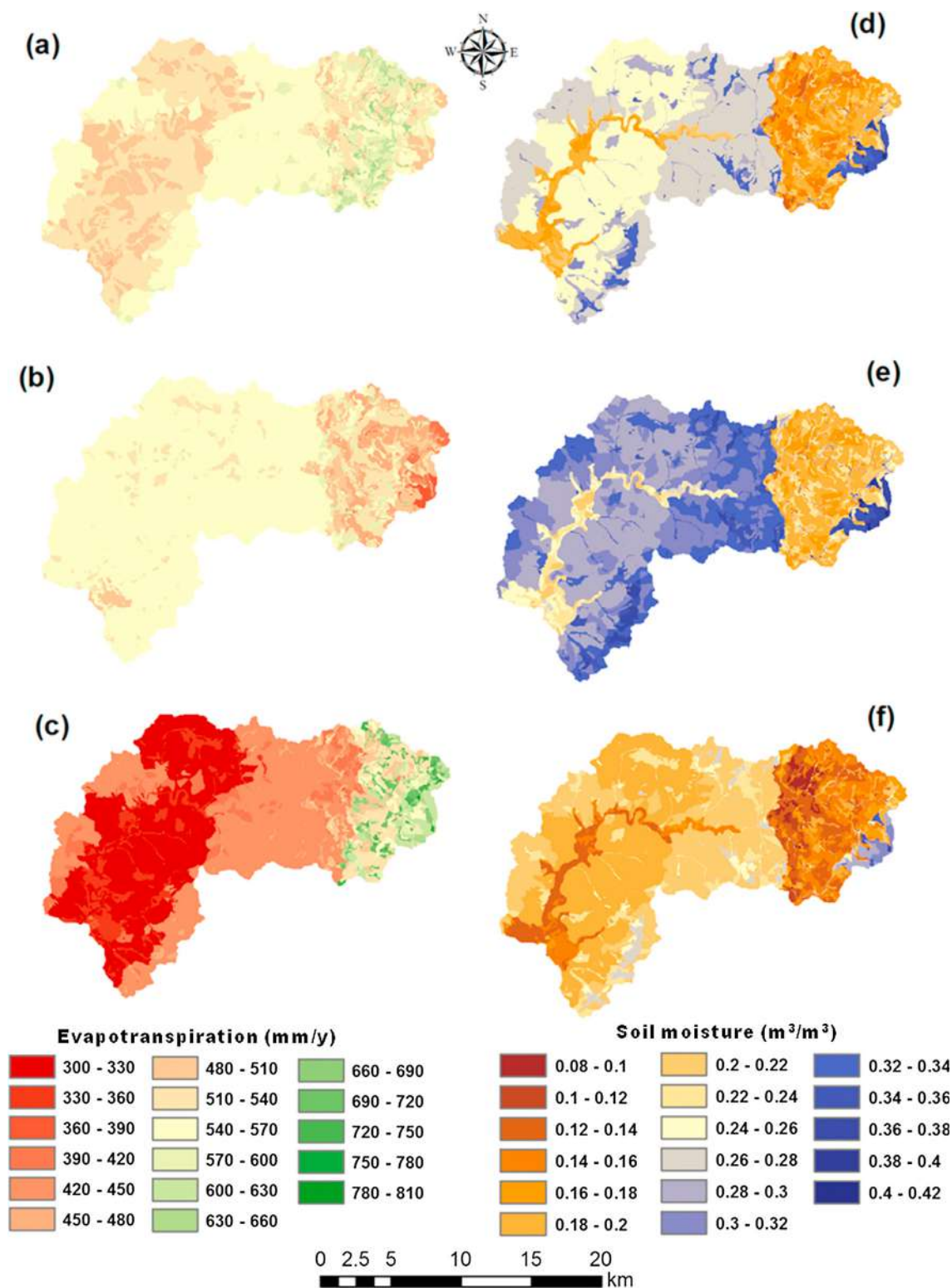The average annual evapotranspiration for the entire study period

Fig. 7. Simulated actual evapotranspiration and soil moisture from the ECS-SLF approach for the McLaughlin catchment, a) average annual evapotranspiration, b) wet year (1978) evapotranspiration, c) dry year (1982) evapotranspiration, d) average soil moisture at surface soil layer for the whole study period (26 yr), e) wet year (1978) average soil moisture at surface soil layer and f) dry year (1982) average soil moisture at surface soil layer.

(1975–2000), wet year (1978) and dry year (1982) from the WaterDyn/ AWAP model are also estimated and presented in Fig. 9a-c. The spatial variation of evapotranspiration of WaterDyn/AWAP model is consistent with the ECS-4LF and ECS-SLF approaches (Figs. 6a-c, 7a-c and 9a-c). The average annual evapotranspiration for 1975–2000 from the Wa- terDyn/AWAP model is higher in the upper part of the catchment and

gradually decreases towards the lower part of the catchment. This spatial pattern is consistent with the spatial pattern of evapo- transpiration from the ECS-4LF and ECS-SLF approaches (Figs. 6a, 7a and 9a).

In the wet year (1978), simulated evapotranspiration from the WaterDyn/AWAP model is higher than the ECS-4LF and ECS-SLF
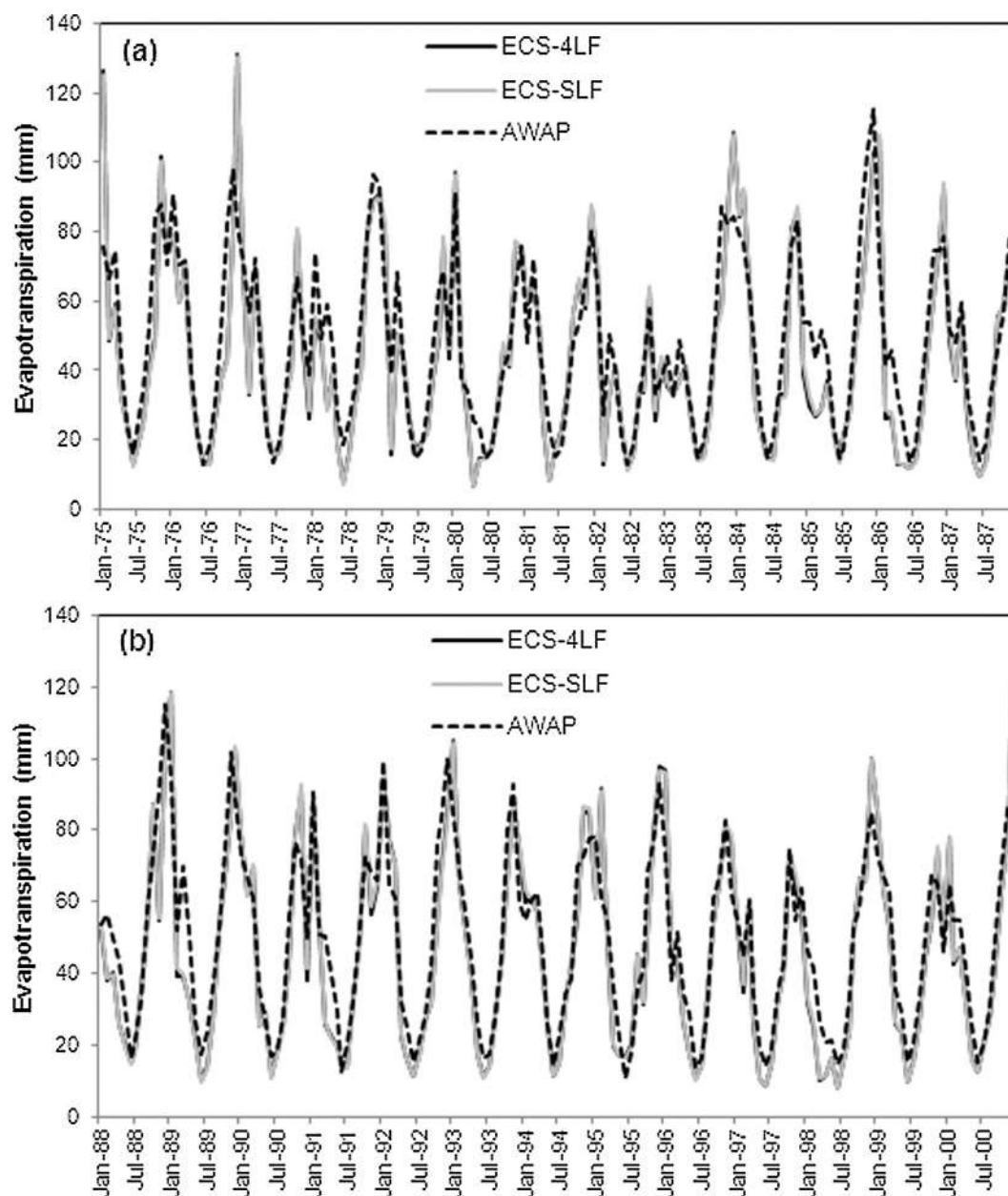
Fig. 8. Comparison of monthly simulated evapotranspiration from the ECS-4LF, ECS-SLF approaches and WaterDyn/AWAP model for the McLaughlin catchment for the period: a) 1975–1987 and b) 1988–2000. Note that the simulated evapotranspiration from the ECS-4LF and ECS-SLF are very close and black and grey lines overlap each other.

approaches as shown in the evapotranspiration time series plot (Figs. 6b, 7b, 8a and 9b). In terms of spatial patterns, simulated evapotranspiration in the upper part of the catchment (where climate zones C & D are located) by the WaterDyn/AWAP are significantly higher (ranges 700 to 790 mm) than the ECS-4LF and ECS-SLF approaches with ranges from 330 to 660 mm (Figs. 1b, 6b, 7b and 9b). The reason for these differences particularly in the wet year is mainly related to the consideration of anoxic conditions in the root zone in U3M-2d model caused by increases in soil saturation.

In the dry year (1982), the spatial pattern of evapotranspiration from the WaterDyn/AWAP model is consistent with the ECS-4LF and ECS-SLF approaches, and all three modelling approaches show higher evapotranspiration in the upper part of the catchment and evapotranspiration is gradually decreasing towards the lower part of the catchment (Figs. 6c, 7c and 9c). In the upper part of the catchment where climate zones C & D are located, the ranges of evapotranspiration

from ECS-4LF and ECS-SLF approaches are high (ranges 360 to 810 mm) compared to the ranges from the WaterDyn/AWAP model (ranges 490 to 580 mm) (Figs. 1b, 6c, 7c and 9c). The reason for these differences is related to differences in soil depth and rooting depth between the two models. In the ECS-4LF and ECS-SLF approaches, soil layers are quite deep and can reach up to 6 m in some areas in the upper part of the catchment. In addition, native woody vegetation has deep rooting depth and can extract water from the deep soil layers (up to 4 m) (Fig. 1c). Whereas in WaterDyn/AWAP model, the maximum depth of soil layer is limited to 1.5 m only and two soil layers are considered with depths of (0 to 0.2 m) and (0.2 to 1.5 m) for the upper and lower soil layers respectively (Raupach et al., 2009). Soil moisture in deep soil layers is high in comparison to the top soil layer as discussed in detail in Sections 4.3 and 4.4.

The mean annual soil moisture from the WaterDyn/AWAP model for the entire study period (1975–2000), wet year (1978) and dry year
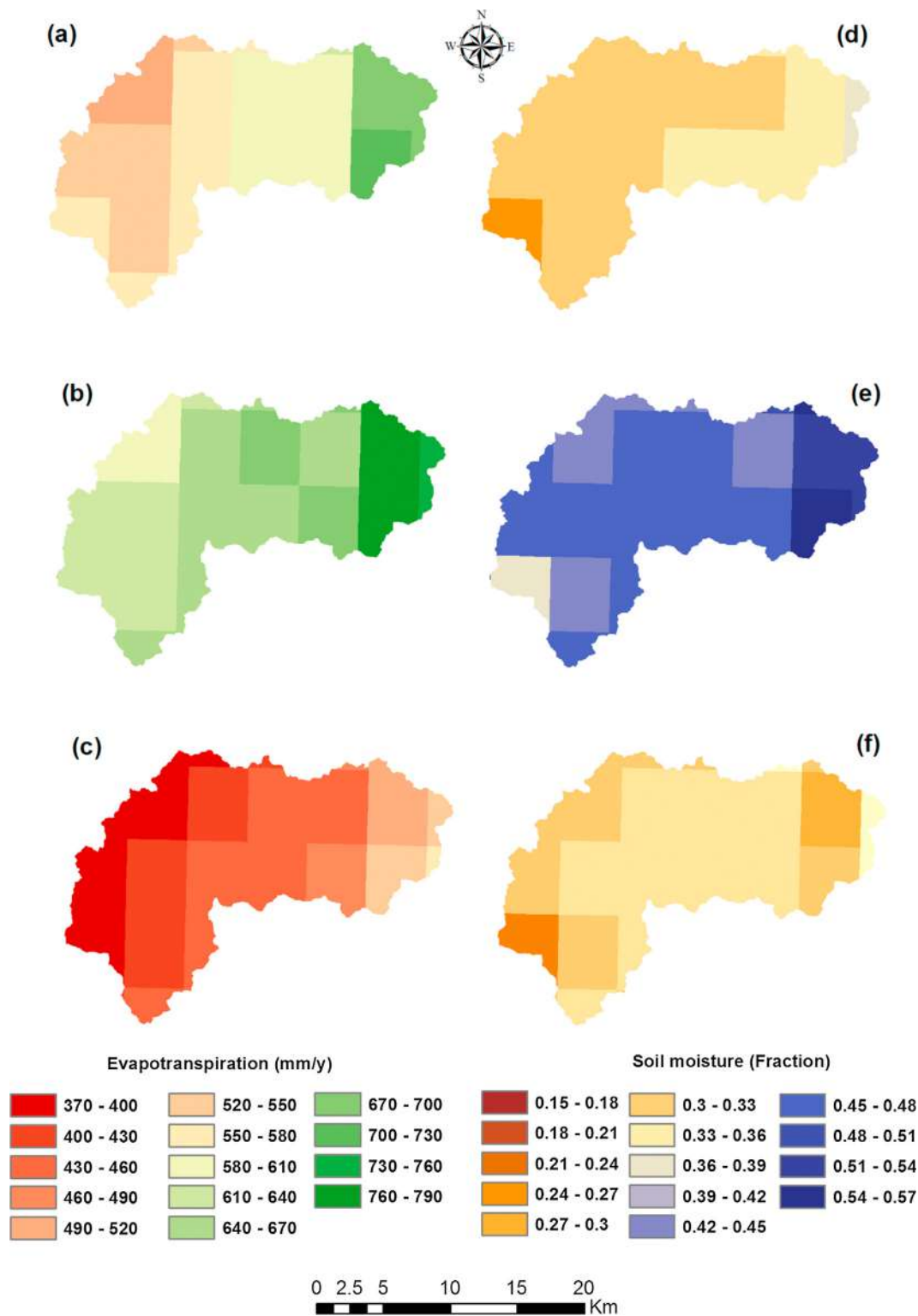
Fig. 9. Simulated actual evapotranspiration and soil moisture from the WaterDyn/AWAP model at 5 km × 5 km grid cells located partly or fully within the McLaughlin catchment, a) average annual evapotranspiration, b) wet year (1978) evapotranspiration, c) dry year (1982) evapotranspiration, d) average soil moisture at upper soil layer for the whole study period (26 yr), e) wet year (1978) average soil moisture at upper soil layer and f) dry year (1982) average soil moisture at upper soil layer.

(1982) are estimated and presented in Fig. 9d-f. In general, horizontal and vertical distribution of soil moisture is highly variable between the two models. Further, the WaterDyn/AWAP model is a daily terrestrial water balance model with a spatial resolution of 5 km × 5 km (Raupach et al., 2009). These limitations make soil moisture comparisons more

challenging. Despite the differences in the spatial resolution of both models, top layer soil moisture patterns in the WaterDyn/AWAP model is consistent with the ECS-4LF and ECS-SLF approaches (Figs. 6d-f, 7d-f and 9d-f). There is a little variation in the upper part of the catchment where ECS-4LF and ECS-SLF approaches show less soil moisture than

Table 4
Correlation coefficient between daily ECS-4LF soil moisture and ESA CCI soil moisture along with the number of ESA CCI observations in each year.

Year	Correlation coefficient	Number of ESA CCI soil moisture data points
1991	0.677	30
1992	0.576	80
1993	0.463	117
1994	0.540	125
1995	0.593	119
1996	0.438	111
1997	0.534	114
1998	0.819	240
1999	0.516	156
2000	0.658	170
1991–2000	0.612	1262

the WaterDyn/AWAP model (Figs. 6d-f, 7d-f and 9d-f). This difference could be caused by the differences in soil properties between the two models. In the ECS-4LF and ECS-SLF approaches, the soil type in the upper part of the catchment is shallow yellow earth granite and earthy sands granite with significantly higher saturated hydraulic conductivity than the deeper soil materials, causing more downward movement of water to the deeper soil materials and lower surface soil moisture (Fig. 1d and Fig. S-2 in Supplementary material). The soil type and properties used in the ECS-4LF and ECS-SLF approaches are from the soil information package of Murphy et al. (2005). These high quality datasets are specifically generated for the McLaughlin and neighbouring catchments in the previous investigations. For the WaterDyn/AWAP model soil properties are obtained from the Digital Atlas of Australian Soils developed at continental scale. Therefore, it is quite likely that soil properties would be different between the two models in some small regions of the catchment. Despite minor differences in the upper part of the catchment, in general the top layer soil moisture spatial pattern from the ECS-4LF and ECS-SLF approaches are comparable with the WaterDyn/AWAP model.

The WaterDyn/AWAP model has been validated for catchment outflows at various time scales in variety of catchments across Australia and few climate variables, and found reasonably accurate (Raupach et al., 2009). Therefore, the WaterDyn/AWAP model outputs are widely used in Australia. Although, there are differences in the input forcings, spatial resolution, modelling methodology and soil information between the WaterDyn/AWAP model and ECS-4LF/ECS-SLF approaches, the simulated evapotranspiration and soil moisture are consistent in most parts of the McLaughlin catchment. These results indicate that the ECS-4LF and ECS-SLF approaches have the potential to simulate evapotranspiration and soil moisture with reasonably good accuracy.

4.2.4. Verification of soil moisture from the European space agency climate change Initiative data set

The correlation coefficients between area weighted catchment average daily surface soil moisture from the ESA CCI and the landform area weighted catchment average daily simulated soil moisture from the ECS-4LF approach are calculated for individual years and the entire period (1991–2000) (Table 4). The correlation coefficient for the entire period is 0.612 but varies for individual year from 0.438 to 0.819 (Table 4) depending on the quality of ESA CCI soil moisture observations in individual years and availability of ESA CCI observations. The average monthly soil moisture is also calculated from the daily catchment average soil moisture from the ESA CCI and ECS-4LF approaches. The correlation coefficient from the average monthly soil moisture for the entire period (1991–2000) is 0.64 which is slightly higher than the daily data. Overall the correlation coefficient values between the two data sets at daily and monthly time scales are reasonably high despite the large differences in spatial resolution.

The ECS-4LF daily soil moisture time series is also compared with the ESA CCI daily soil moisture time series for year 1995 in Fig. 10 as the same year is used for streamflow comparison (Fig. 4). The simulated soil moisture values from the ECS-4LF approach are matching closely with the ESA CCI soil moisture values (Fig. 10). Similar trends are also observed in other years. Considering the large differences in horizontal as well as vertical resolution between the ECS-4LF and ESA CCI approaches, the soil moisture values from both approaches are close. This result indicates that the simulated soil moisture from the ECS-4LF is reasonably accurate and reliable considering that no calibration is performed in the ECS-4LF approach. As ECS-4LF is the best performing approach, no comparison with the ECS-SLF is performed.
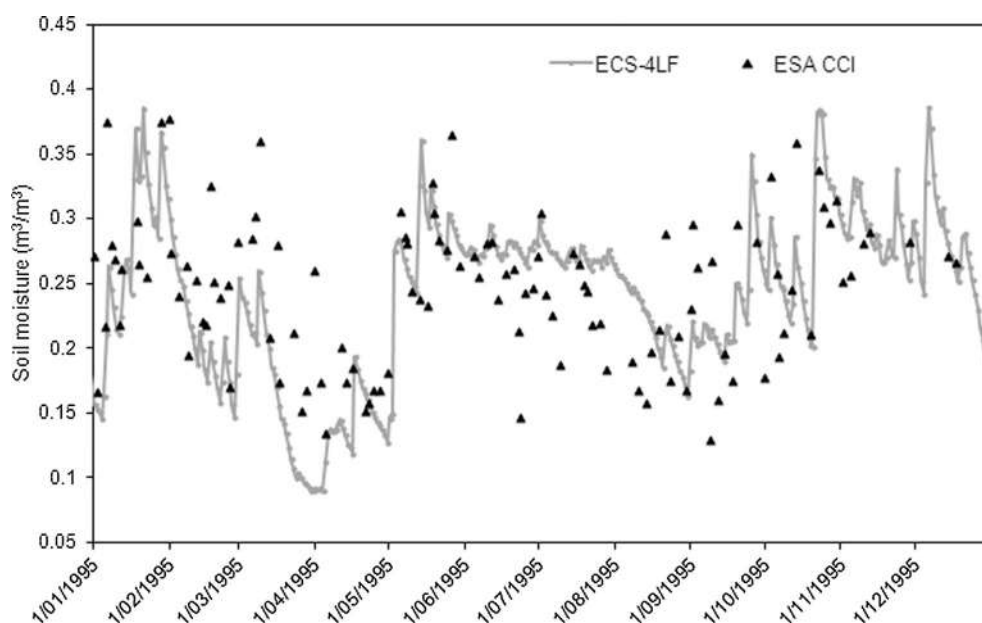

Fig. 10. Comparison of daily catchment average simulated soil moistures from the ECS-4LF approach with satellite derived ESA CCI daily catchment average soil moisture for the year 1995.
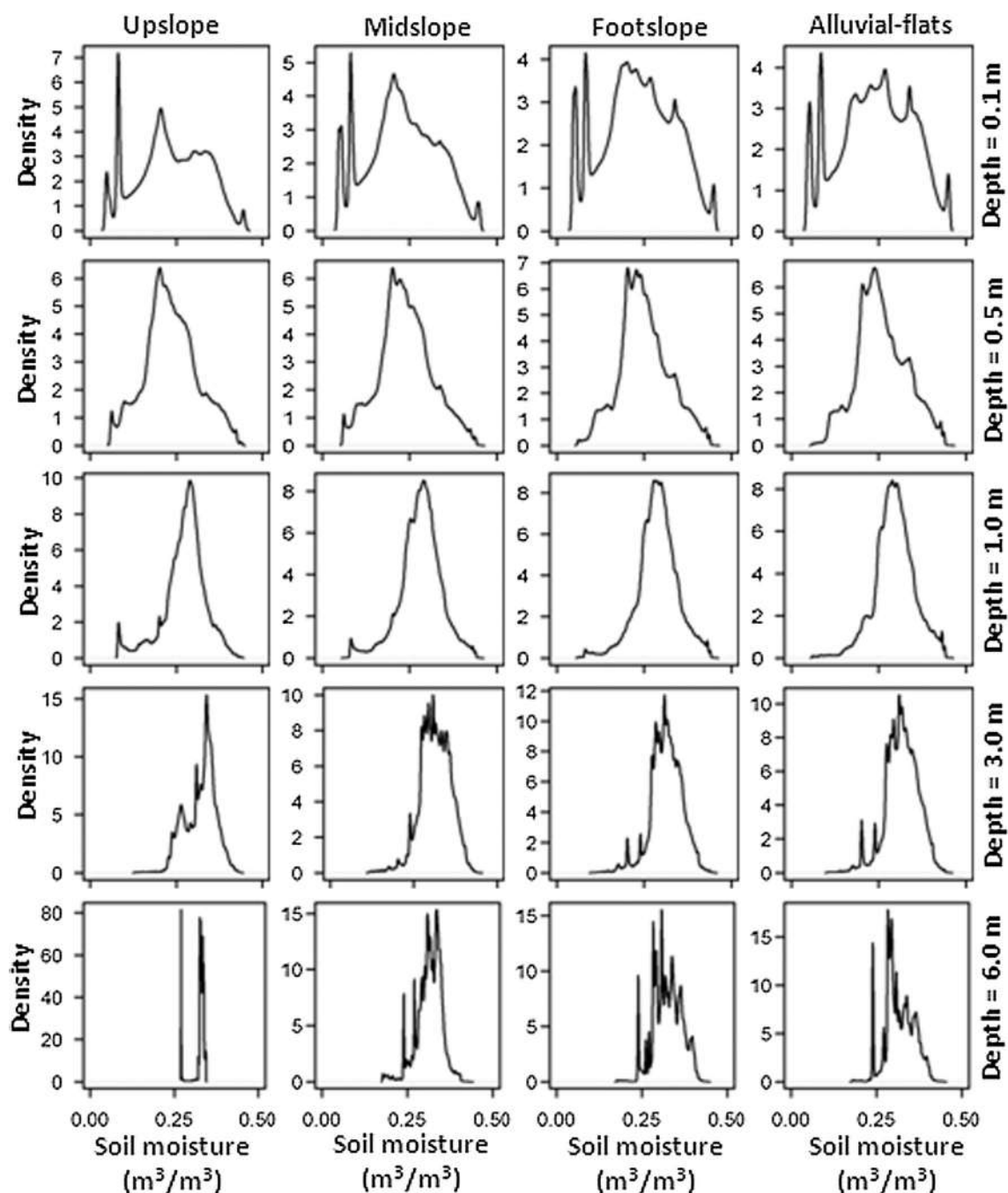
Fig. 11. Kernel density plots showing the distribution of daily soil moisture across four landforms at different soil depths in the ECS-4LF approach for the McLaughlin catchment.

4.3. Vertical distribution of soil moisture across different landforms

The vertical distribution of soil moisture is important for calculating the soil moisture deficit for irrigation purposes. To analyze the vertical soil moisture distribution across the landforms in ECS-4LF approach, the Kernel density and bar plots of soil moisture are presented for various soil depths and four landforms of the entire McLaughlin catchment (Figs. 11 & 12). To obtain the Kernel density plots, pixel based values of daily soil moisture at a particular depth are averaged for a given landform across the catchment (Fig. 11). Note that to avoid excessive number of Kernel density plots in Fig. 11, data for a few nodal soil depths are shown. Fig. 12a-b shows the mean and standard deviation of daily soil moisture for each landform at various soil depths.

Kernel density and bar plots show the variation of soil moisture in four landforms at various depths for the entire McLaughlin catchment (Figs. 11 & 12). Overall, soil moisture variability is highest at the surface soil layer, i.e., at 10 cm depth, for all the landforms; however mean soil moisture is low, due to high transpiration and soil evaporation. Soil moisture variability reduces in deeper soil layers because of lower permeability of deep soil layers which restrict soil water movement. Soil evaporation and transpiration from deep soil layers are negligible because of the lower permeability of deep soil layers and shallow rooting depth of pasture (Figs. 11 & 12). Note: the pasture is dominant land cover type in the McLaughlin catchment (Fig. 1c). The Kernel density plots of all the landforms, at various soil depths (0.1, 0.5, 1.0, 3.0 & 6.0 m), clearly show shift of the distribution plots towards the right side as depth increases (Fig. 11), i.e., increase in mean soil moisture at deeper soil layers (Fig. 12a). The Kernel density plots are
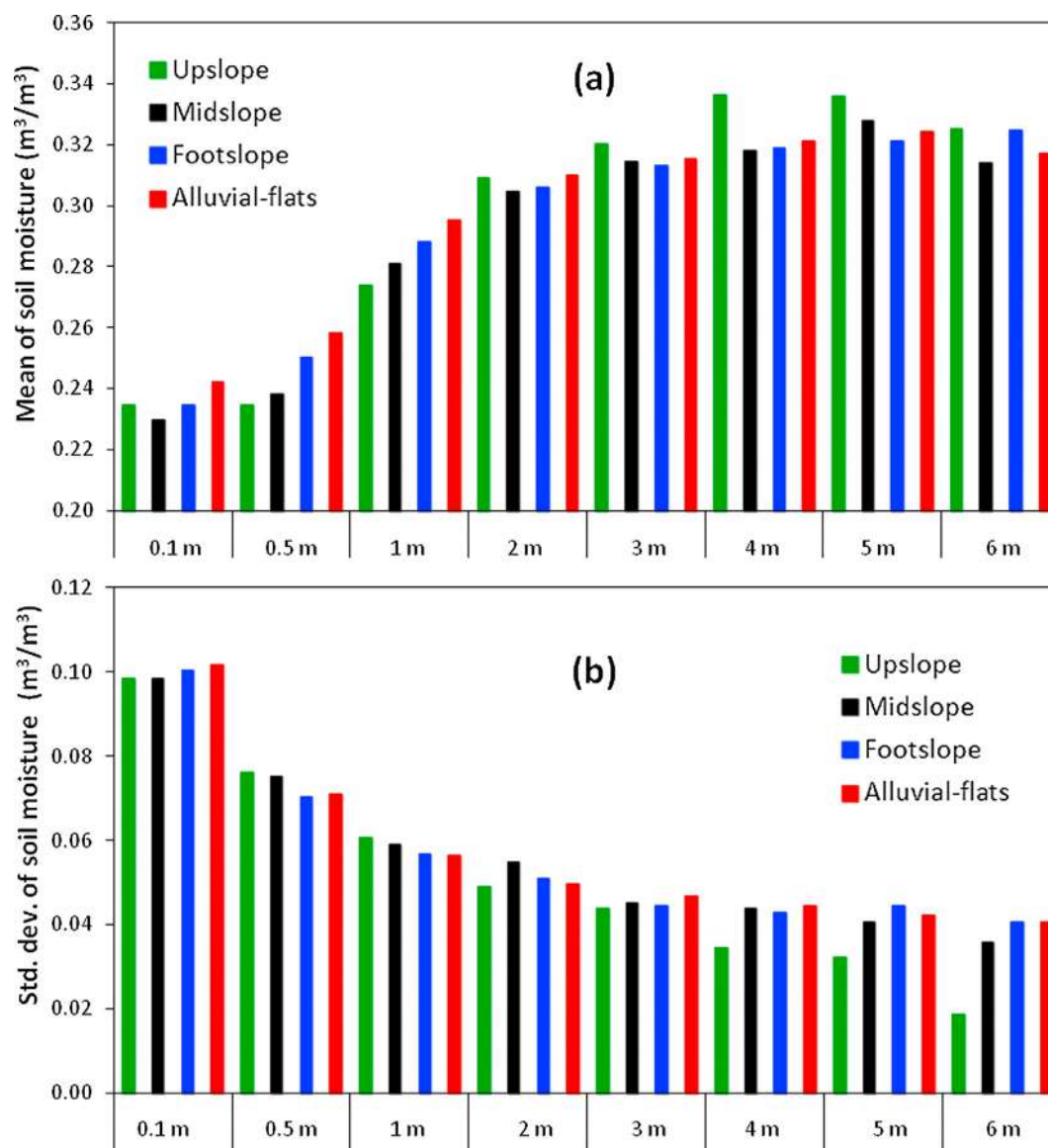
Fig. 12. Bar plots showing the a) mean and b) standard deviation of daily soil moisture across four landforms in the ECS-4LF approach at different soil depths for the McLaughlin catchment.

spiky at 3.0 m and 6.0 m depths (Fig. 11), as the number of simulated data points is less at higher soil depths. Note that the soil depths are not constant throughout the catchment. Generally, upper parts of the hillslopes have shallower soils and the thickness of soil zone gradually increases towards the lower part of the hillslopes. The mean soil moisture is increasing from 0.1 m to 1.0 m depth within four landforms, i.e., upslope to alluvial-flats, due to more saturation near the river network. After 1.0 m depth, the mean soil moisture is almost constant in all four landforms because deeper soil layers are wetter (Fig. 12a).

The simulated soil moisture at 15 cm depth from the ECS approach was thoroughly validated against in-situ soil moisture for Wagga-Wagga experimental catchment by Khan et al. (2014) indicating reasonable accuracy of soil moisture simulations by the ECS approach. Further, the soil moisture at various soil depths in this study is also consistent with the input forcing and follows the expected behaviour.

As ECS-SLF approach only contains one single landform in a soil polygon therefore above mentioned analysis cannot be performed for ECS-SLF approach.

4.4. Impact of different climate and land cover on soil moisture

To analyze the impact of different climate and land cover on soil moisture values on four landforms at various soil depths, the Kernel density and bar plots of mean and standard deviation are explored for ECS-4LF approach. To avoid an excessive number of plots only mean plots are presented in Fig. 13a-b. Other plots are available from the authors on request. Two extreme climate zones, wettest (zone-D) and driest (zone-A) are considered. The mean soil moisture values of each landform at various soil depths are calculated for ECS-4LF approach in a similar manner as calculated in section-4.3. However, the averaging is performed at the scale of individual climate zones rather than the entire catchment (Fig. 13a). As it is expected, mean soil moisture in zone A (driest zone) is lower than zone D throughout all landforms and soil depths (Fig. 1b). Despite the large differences in the mean annual rainfall in the climate zones A & D (551 mm/y vs. 1300 mm/y), the same order of differences is not reflected in soil moisture values in Fig. 13a. This is because the soil hydraulic properties as well as the land cover types play an important role in controlling the soil moisture in the catchment. In the case of climate zone D, a major part of this region is
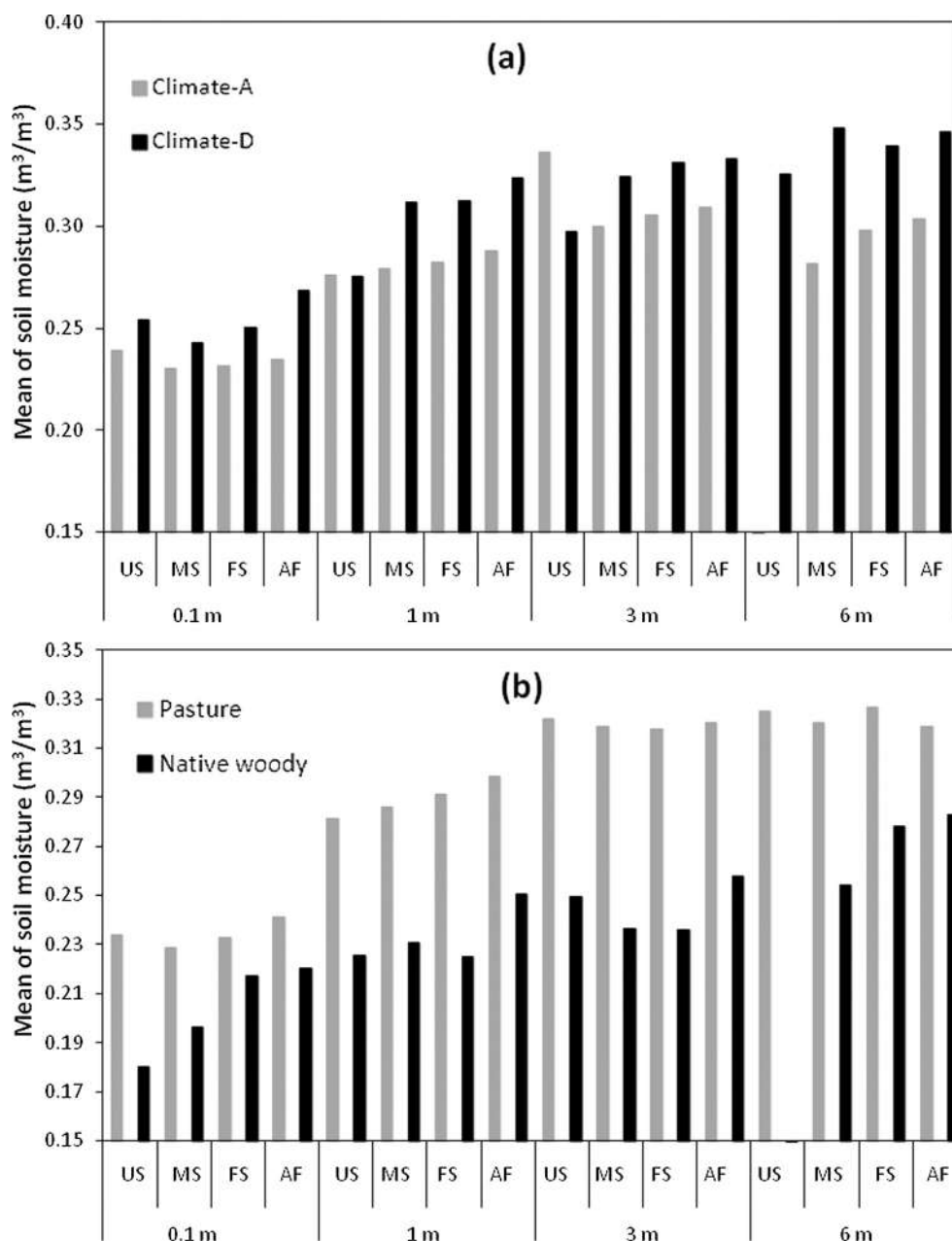
Fig. 13. Role of a) two extreme climatic zones (zone A dry & D wet) and b) land cover types (pasture and native woody) on vertical distribution of mean daily soil moisture at selected depths across four landforms within the McLaughlin catchment using the ECS-4LF approach. US, MS, FS and AF stand for landform-upslope, -midslope, -footslope and -alluvial-flats.

covered with highly permeable soils that allow more deep drainage. In addition, presence of native woody land cover type in this area causes high transpiration rates (Fig. 1b-d and Fig. S-2 in Supplementary material). The impact of transpiration and soil evaporation on soil moisture diminishes at 6.0 m depth, whereas substantial differences exist in mean soil moisture between climate zones A & D.

The mean soil moistures of four landforms at various soil depths are calculated separately for ECS-4LF approach for both land cover types, i.e., pasture and native woody, using the same methodology as used for climate zones (Fig. 13b). The mean soil moisture values for native woody are consistently lower than the pasture across all landforms and soil depths. Higher transpiration from native woody is caused by deep rooting depth (the maximum root depth for pasture is 60 cm, whereas for native woody is 4.0 m) and access to deeper soil moisture. The soil hydraulic properties are also playing an important role in reducing the soil moisture in native woodlands. The native woodlands are located in

the areas where soil types have higher saturated hydraulic conductivity which causes more deep drainage (Fig. 1c-d and Fig. S-2 in Supplementary material). Note that, in Fig. 13a the mean soil moisture values in climate zone A for upslope at 6.0 m soil depth is not shown. This is because the simulated soil moisture data is not available at this depth in climate zone A for upslope. In a similar manner, the simulated soil moisture data is not available for native woody in upslope at 6.0 m soil depth (Fig. 13b).

The soil moisture information at various soil depths in each land cover types is very helpful for calculating soil moisture deficit for irrigation purposes. Note that, the above mentioned analysis cannot be performed for the ECS-SLF approach as a single landform exists in each soil polygon. Implementation of the ECS-4LF approach is recommended over the ECS-SLF approach because the ECS-4LF disaggregates the hillslope realistically and provides more information about spatial variability of soil moisture and hydrologic fluxes.

5. Summary

The ECS approach developed previously by Khan et al. (2014) was applicable at the first order sub-basin scale, whereas the presented ECS-4LF approach is modified to apply at the catchment scale. We made some simplifications for automating the presented ECS-4LF delineation approach for catchment scale applications. The simulated discharge from the modified ECS-4LF based distributed modelling approach without calibration shows reasonable consistency with the observed streamflow and all lumped conceptual models used in this study. This consistency indicates that the ECS-4LF approach has the potential to be applied for distributed modelling of other catchments especially un-gauged catchments where observed streamflow data are not available or not sufficient for proper calibration of the conceptual models. The ECS-4LF modelling approach along with the 2-d Richards' equation makes this approach more suitable for simulating the shallow sub-surface flows in upland catchments. Like other distributed hydrologic models, the ECS-4LF approach also requires extensive spatial input data, i.e., DEM, soil type, land cover, climate and geology to derive model parameters. Currently, the ECS-4LF approach is used in research mode. Further development and evaluation are required in variety of settings to make it an operational product. Future developments are focused on developing a Graphical User Interface (GUI) for automating ECS-4LF delineation, development of groundwater and detailed eco-hydrological modules. Despite these limitations, the presented ECS-4LF approach is a valuable tool for simulating spatially distributed hydrological fluxes with high accuracy, and significantly reducing the computational time/units associated with typical distributed hydrological modelling applications.

6. Conclusions

An equivalent cross-section based semi-distributed hydrologic modelling approach initially developed for eight discrete first order sub-basins, is modified here for a large catchment scale simulation containing 822 first order sub-basins. All parameters used in this approach are derived from the actual topographical and physiographical features of the catchment without any calibration or adjustment being needed. The simulated streamflows from the equivalent cross-section approach are consistent with the observed streamflows. The simulated streamflows are also compared with four calibrated conceptual models' streamflows and results found to be comparable. In addition, the equivalent cross-section approach shows nearly a 40 times reduction in computational units when compared to a grid based fully distributed hydrological modelling setup. Performance of the ECS-4LF was better than the ECS-SLF approach considering that the ECS-4LF represents the spatial variability of hydrologic fluxes along the hillslope. The simulated actual evapotranspiration and soil moisture from the ECS-4LF and ECS-SLF approaches are very similar to the AWAP model. Further, the simulated soil moisture from the ECS-4LF approach is found to be consistent with the satellite derived European Space Agency Climate Change Initiative (ESA CCI) surface soil moisture data.

The equivalent cross-section based semi-distributed modelling approach has the ability to simulate variety of spatially distributed hydrological fluxes that are consistent with the input forcing and land surface characteristics. The results at the landform scale show that within the landforms, the mean soil moisture in shallow layers has increased as we move from upslope to alluvial-flats due to the saturation near river network. This pattern is not significant in small regions in lower parts of the catchment especially along the main stem of the river network because of low soil moisture values in all landforms. In deeper soil layers, the mean soil moisture is almost constant across all landforms due to low saturated hydraulic conductivity. The variability in soil moisture is higher for surface soil layers due to high evapotranspiration and lower for deeper soil layers for all landforms. The pasture dominated region of the catchment has higher soil moisture

than the native woody due to shallower root depths and lower LAI.

It can be concluded that the equivalent cross-section based semi-distributed hydrological modelling has the potential to simulate a variety of hydrological fluxes for a large catchment in a computationally efficient manner while maintaining accuracy with respect to the observed streamflow and consistency with the input forcings.

Appendix A. Supplementary data

Supplementary data associated with this article can be found, in the online version, at https://doi.org/10.1016/j.jhydrol.2018.07.066.

References

Abbott, M.B., Bathurst, J.C., Cunge, J.A., O'Connell, P.E., Rasmussen, J., 1986a. An introduction to the European Hydrological System — Systeme Hydrologique Europeen, "SHE", 1: history and philosophy of a physically-based, distributed modelling system. J. Hydrol. 87 (1–2), 45–59.

Abbott, M.B., Bathurst, J.C., Cunge, J.A., O'Connell, P.E., Rasmussen, J., 1986b. An introduction to the European Hydrological System — Systeme Hydrologique Europeen, "SHE", 2: structure of a physically-based, distributed modelling system. J. Hydrol. 87 (1–2), 61–77.

Abbott, M.B., Refsgaard, J.C., 1996. Distributed Hydrological Modelling. Kluwer Academic Pub.

Ajami, H., Khan, U., Tuteja, N.K., Sharma, A., 2016. Development of a computationally efficient semi-distributed hydrologic modeling application for soil moisture, lateral flow and runoff simulation. Environ. Modell. Software 85, 319–331.

Argent, R.M., Podger, G.M., Grayson, R.B., Fowler, K., Murray, N., 2007. E2 Catchment Modelling Software, eWater. Cooperative Research Centre for Catchment Hydrology, Australia.

Bell, V.A., Kay, A.L., Jones, R.G., Moore, R.J., 2007. Development of a high resolution grid-based river flow model for use with regional climate model output. Hydrol. Earth Syst. Sci. 11 (1), 532–549.

Beven, K., 1989. Changing ideas in hydrology — The case of physically-based models. J. Hydrol. 105 (1–2), 157–172.

Beven, K., 2001. How far can we go in distributed hydrological modelling? Hydrol. Earth Syst. Sci. 5 (1), 1–12.

Beven, K., 2012. Rainfall-runoff Modelling: The Primer. Wiley-Blackwell, Chichester.

Beven, K.J., Kirkby, M.J., 1979. A physically based, variable contributing area model of basin hydrology. Hydrol. Sci. J. 24 (1), 43–69.

Brunner, P., Simmons, C.T., 2012. HydroGeoSphere: a fully integrated, physically based hydrological model. Ground Water 50 (2), 170–176.

Burnash, R.J., 1985. The Sacramento watershed model, hydrologic modelling for flood hazards, Hydrologic Modelling for Flood Hazards Planning and Management, University of Colorado at Denver, California-Nevada River Forecast Center, National Weather Service, Sacramento.

Burnash, R.J.C., Ferral, R.L., McGuire, R.A., 1973. A generalized streamflow simulation system: conceptual modeling for digital computers. U. S. Dept. of Commerce, National Weather Service.

Chapman, G.A., Atkinson, G., 2000. Soil survey and mapping. In: Charman, P.E.V., Murphy, B.W. (Eds.), Soils – Their Properties and Management. Oxford University Press.

Chiew, F.H.S., Peel, M.C., Western, A.W., 2002. Application and testing of the simple

rainfall-runoff model SIMHYD. In: Singh, V.P., Frevert, D.K. (Eds.), Mathematical Models of Small Watershed Hydrology and Applications Littleton. Water Resources Publication, Colorado.

Chung, D., Dorigo, W., De Jeu, R., Kidd, R., Wagner, W., 2018. ESA Climate Change Initiative Phase II - Soil Moisture, Product Specification Document (PSD) D1.2.1 Version 4.2, Earth Observation Data Centre for Water Resources Monitoring (EODC) GmbH.

Cole, S.J., Moore, R.J., 2009. Distributed hydrological modelling using weather radar in gauged and ungauged basins. Adv. Water Resour. 32 (7), 1107–1120.

Cunge, J.A., 1969. On the subject of a flood propagation computation method (Musklngum Method). J. Hydraul. Res. 7 (2), 205–230.

Dorigo, W., et al., 2017. ESA CCI Soil Moisture for improved Earth system understanding: state-of-the art and future directions. Remote Sens. Environ. 203, 185–215.

Downer, C.W., Ogden, F.L., 2004. GSSHA: model to simulate diverse stream flow producing processes. J. Hydrol. Eng. 9 (3), 161–174.

Duan, Q.Y., Gupta, V.K., Sorooshian, S., 1993. Shuffled complex evolution approach for effective and efficient global minimization. J. Optim. Theory Appl. 76 (3), 501–521.

Duan, Q.Y., Sorooshian, S., Gupta, V.K., 1994. Optimal use of the SCE-UA global optimization method for calibrating watershed models. J. Hydrol. 158 (3), 265–284.

Flugel, W.A., 1995. Delineating Hydrological Response Units by Geographical Information system analyses for regional Hydrological Modelling using PRMS/MMS in the drainage basin of the river Brol, Germany. Hydrol. Processes 9 (3–4), 423–436.

Geeves, G.W., Cresswell, H.P., Murphy, B.W., Gessler, P.E., Chartres, C.J., Little, I.P., Bowman, G.M., 1995. The physical, chemical, and morphological properties of soils in the wheat belt of southern NSW and northern Victoria., NSW Department of Conservation and Land Management/CSIRO Australia. Division of Soils Occasional report.

Grayson, R.B., Moore, I.D., McMahon, T.A., 1992a. Physically based hydrologic modeling: 1. A terrain-based model for investigative purposes. Water Resour. Res. 28 (10), 2639–2658.

Grayson, R.B., Moore, I.D., McMahon, T.A., 1992b. Physically based hydrologic modeling: 2. Is the concept realistic? Water Resour. Res. 28 (10), 2659–2666.

Ivanov, V.Y., Bras, R.L., Vivoni, E.R., 2008a. Vegetation-hydrology dynamics in complex terrain of semiarid areas: 1. A mechanistic approach to modeling dynamic feedbacks. Water Resour. Res. 44 (3), 34.

Ivanov, V.Y., Bras, R.L., Vivoni, E.R., 2008b. Vegetation-hydrology dynamics in complex terrain of semiarid areas: 2. Energy-water controls of vegetation spatiotemporal dynamics and topographic niches of favorability. Water Resour. Res. 44 (3), 20.

Jeffrey, S.J., Carter, J.O., Moodie, K.B., Beswick, A.R., 2001. Using spatial interpolation to construct a comprehensive archive of Australian climate data. Environ. Modell. Software 16 (4), 309–330.

Kachroo, R.K., 1992. River flow forecasting, Part 5: Applications of a conceptual model. J. Hydrol. 133, 141–178.

Kampf, S.K., Burges, S.J., 2007. A framework for classifying and comparing distributed hillslope and catchment hydrologic models. Water Resour. Res. 43 (5).

Kavetski, D., Kuczera, G., Franks, S.W., 2006a. Bayesian analysis of input uncertainty in hydrological modeling: 1. Theory. Water Resources Research 42 (3), W03407.

Kavetski, D., Kuczera, G., Franks, S.W., 2006b. Bayesian analysis of input uncertainty in hydrological modeling: 2. Application. Water Resour. Res. 42 (3), W03408.

Khan, U., Tuteja, N.K., Ajami, H., Sharma, A., 2014. An equivalent cross-sectional basis for semidistributed hydrological modeling. Water Resour. Res. 50 (5), 4395–4415.

Khan, U., Tuteja, N.K., Sharma, A., 2013. Delineating hydrologic response units in large upland catchments and its evaluation using soil moisture simulations. Environ. Modell. Software 46 (2013), 142–154.

Kim, S., Paik, K., Johnson, F.M., Sharma, A., 2018. Building a flood-warning framework for ungauged locations using low resolution, open-access remotely sensed surface soil moisture, precipitation, soil, and topographic information. IEEE J. Sel. Top. Appl. Earth Observations Remote Sensing 11, 375–387.

Kirchner, J.W., 2006. Getting the right answers for the right reasons: Linking measurements, analyses, and models to advance the science of hydrology. Water Resour. Res. 42 (3), W03S04.

Knudsen, J., Thomsen, A., Refsgaard, J.C., 1986. WATBAL - A Semi-distributed, physically based hydrological modeling system. Nord. Hydrol. 17 (4–5), 347–362.

Kollet, S.J., Maxwell, R.M., 2006. Integrated surface-groundwater flow modeling: A freesurface overland flow boundary condition in a parallel groundwater flow model. Adv. Water Resour. 29 (7), 945–958.

Liang, G.C., Nash, J.E., 1988. Linear models for river flow routing on large catchments. J. Hydrol. 103 (1–2), 157–188.

Liu, Y.Y., Dorigo, W.A., Parinussa, R.M., De Jeu, R.A.M., Wagner, W., McCabe, M.F., Evans, J.P., Van Dijk, A.I.J.M., 2012. Trend-preserving blending of passive and active microwave soil moisture retrievals. Remote Sens. Environ. 123, 280–297.

McKenzie, N.J., Gallant, J.C., Gregory, L.J., 2003. Estimating Water Storage Capacities in Soil at Catchment Scales, Technical Report 03/3. Research for Catchment Hydrology, Australia.

Minasny, B., McBratney, A.B., 2002. The neuro-m method for fitting neural network parametric pedotransfer functions. Soil Sci. Soc. Am. J. 66 (2), 352–361.

Miralles, D.G., van den Berg, M.J., Gash, J.H., Parinussa, R.M., de Jeu, R.A.M., Beck, H.E., Holmes, T.R.H., Jiménez, C., Verhoest, N.E.C., Dorigo, W.A., Teuling, A.J., Dolman, Johannes, 2013. El Niño–La Niña cycle and recent trends in continental evaporation. Nat. Clim. Change 122, 122.

Murphy, B., Young, J., Vaze, J., Teng, J., Jenkins, B., Summerell, G., Townsend, F., 2005. Soils information package to support the development of the snowy Monaro landscape plantation strategy: a report on the methodology to develop the soils information package. Department of Natural Resources, NSW, Australia.

Nash, J.E., 1959. A note on the Muskingum flood-routing method. J. Geophys. Res. 64 (8), 1053–1056.

Nash, J.E., Barsi, B.I., 1983. A hybrid model for flow forecasting on large catchments. J. Hydrol. 65 (1–3), 125–137.

Nash, J.E., Sutcliffe, J.V., 1970. River flow forecasting through conceptual models Part 1, A discussion of principles. J. Hydrol. 10, 282–290.

Nielsen, S.A., Hansen, E., 1973. Numerical simulation of the rainfall-runoff process on a daily basis. Nord. Hydrol. 4, 171–190.

O'Connell, P.E., Nash, J.E., Farrell, J.P., 1970. River flow forecasting through conceptual models part II – The Brosna catchment at Ferbane. J. Hydrol. 10, 317–329.

Panday, S., Huyakorn, P.S., 2004. A fully coupled physically-based spatially-distributed model for evaluating surface/subsurface flow. Adv. Water Resour. 27 (4), 361–382.

Paniconi, C., Marrocu, M., Putti, M., Verbunt, M., 2003. Newtonian nudging for a Richards equation-based distributed hydrological model. Adv. Water Resour. 26 (2), 161–178.

Perrin, C., Michel, C., Andréassian, V., 2003. Improvement of a parsimonious model for streamflow simulation. J. Hydrol. 279 (1–4), 275–289.

Podger, G.M., 2004. RRL Rainfall-Runoff Library, User Guide. Cooperative Research Centre for Catchment Hydrology, Australia.

Raupach, M.R., Briggs, P.R., Haverd, V., King, E.A., Paget, M., Trudinger, C.M., 2009. Australian Water Availability Project (AWAP): CSIRO Marine and Atmospheric Research Component: Final Report for Phase 3, Centre for Australian Weather and Climate Research (CAWCR), a Partnership between the Bureau of Meteorology and CSIRO, Melbourne, Australia.

Reed, S., Koren, V., Smith, M., Zhang, Z., Moreda, F., Seo, D.-J., Dmip Participants, 2004. Overall distributed model intercomparison project results. J. Hydrol. 298 (1–4), 27–60.

Refsgaard, J.C., Knudsen, J., 1996. Operational validation and intercomparison of different types of hydrological models. Water Resour. Res. 32 (7), 2189–2202.

Reggiani, P., Hassanizadeh, S.M., Sivapalan, M., Gray, W.G., 1999. A unifying framework for watershed thermodynamics: constitutive relationships. Adv. Water Resour. 23 (1), 15–39.

Reggiani, P., Sivapalan, M., Hassanizadeh, S.M., 1998. A unifying framework for watershed thermodynamics: balance equations for mass, momentum, energy and entropy, and the second law of thermodynamics. Adv. Water Resour. 22 (4), 367–398.

Schaap, M.G., Leij, F.J., 1998. Database-related accuracy and uncertainty of pedotransfer functions. Soil Sci. 163 (10), 765–779.

Shin, D., Schepen, A., Peatey, T., Zhou, S., MacDonald, A., Chia, T., Perkins, J., Plummer, N., 2011. WAFARi: A new modelling system for Seasonal Streamflow Forecasting service of the Bureau of Meteorology, Australia. In: Chan, F., Marinova, D., Anderssen, R.S. (Eds.), 19th International Congress on Modelling and Simulation, Perth, Australia, pp. 2374–2380.

Simunek, J., Sejna, M., van Genuchten, M.T., 1999. The HYDRUS-2D software package for simulating two-dimensional movement of water, heat, and multiple solutes in variably saturated media, Int. Ground Water Model. Cent., Colo. Sch. of Mines, Golden.

Simunek, J., van Genuchten, M.T., Sejna, M., 2005. The HYDRUS-1D software package for simulating the movement of water, heat, and multiple solutes in variably saturated media, version 3.0, Dep. of Environ. Sci., Univ. of Calif., Riverside.

Simunek, J., van Genuchten, M.T., Sejna, M., 2006. The HYDRUS software package for simulating two- and three-dimensional movement of water, heat, and multiple solutes in variably-saturated media, version 1.0, technical manual, PC Progress, Prague, Czech Republic.

Singh, V.P., 1995. Computer models of watershed hydrology. Water Resources Publications, Highlands Ranch, Colo.

Singh, V.P., Woolhiser, D.A., 2002. Mathematical modeling of watershed hydrology. J. Hydrol. Eng. 7 (4), 270–292.

Summerell, G.K., Vaze, J., Tuteja, N.K., Grayson, R.B., Beale, G., Dowling, T.I., 2005. Delineating the major landforms of catchments using an objective hydrological terrain analysis method. Water Resour. Res. 41 (12), 1–12.

Tague, C.L., Band, L.E., 2004. RHESSys: regional hydro-ecologic simulation system—An object-oriented approach to spatially distributed modeling of carbon, water, and nutrient cycling. Earth Interact. 8 (19), 1–42.

Teng, J., Vaze, J., Tuteja, N.K., Gallant, J.C., 2008. A GIS based tool for spatial and distributed hydrological modelling: CLASS Spatial Analyst. Trans. GIS 12, 209–225.

Tuteja, N.K., Cunnane, C., 1999. A quasi physical snowmelt runoff modelling system for small catchments. Hydrol. Process. 13, 1961–1975.

Tuteja, N.K., Shin, D., Laugesen, R., Khan, U., Shao, Q., Wang, E., Li, M., Zheng, H., Kuczera, G., Kavetski, D., Evin, G., Thyer, M., MacDonald, A., Chia, T., Le, B., 2011. Experimental evaluation of the dynamic seasonal streamflow forecasting approach. Bureau of Meteorology, Melbourne.

Tuteja, N.K., Vaze, J., Murphy, B., Beale, G.T.B., 2004. CLASS: Catchment Scale Multiple-Landuse Atmosphere Soil Water and Solute Transport Model. Cooperative Research Centre for Catchment Hydrology, Canberra, Australia.

Tuteja, N.K., Vaze, J., Teng, J., Murphy, B.W., Mutendeudzi, M., 2006. Impact of pine plantations on runoff from the snowy catchment. A report on outcomes from hydrological modelling work to support landscape strtegy for the snowy Monaro region, Department of Natural Resources New South Wales, Canberra.

Tuteja, N.K., Vaze, J., Teng, J., Mutendeudzi, M., 2007. Partitioning the effects of pine plantations and climate variability on runoff from a large catchment in southeastern Australia. Water Resour. Res. 43 (8), W08415.

Vaze, J., Tuteja, N.K., Teng, J., 2004. CLASS Unsaturated Moisture Movement Model U3M-1D, User's Manual, NSW Department of Infrastructure, Planning and Natural Resources, Sydney, Australia.

Vertessy, R.A., Hatton, T.J., O'Shaughnessy, P.J., Jayasuriya, M.D.A., 1993. Predicting water yield from a mountain ash forest catchment using a terrain analysis based catchment model. J. Hydrol. 150 (2–4), 665–700.

Watson, F.G.R., Grayson, R.B., Vertessy, R.A., McMahon, T.A., 1998. Large-scale distribution modelling and the utility of detailed ground data. Hydrol. Process. 12 (6),

873–888.

Watson, F.G.R., Vertessy, R.A., Grayson, R.B., 1999. Large-scale modelling of forest hydrological processes and their long-term effect on water yield. Hydrol. Process. 13 (5), 689–700.

Wigmosta, M.S., Vail, L.W., Lettenmaier, D.P., 1994. A distributed hydrology-vegetation model for complex terrain. Water Resour. Res. 30 (6), 1665–1679.

Wood, E.F., Sivapalan, M., Beven, K., Band, L., 1988. Effects of spatial variability and scale with implications to hydrologic modeling. J. Hydrol. 102 (1–4), 29–47.